Noname manuscript No.
(will be inserted by the editor)

Small Specimen Techniques for Estimation of Tensile, Fatigue, Fracture and Crack Propagation Material Model Parameters

J. Kazakeviciute · J. P. Rouse · D. S. A. De Focatiis · C. J. Hyde

Received: date / Accepted: date

Abstract Small specimen mechanical testing is an exciting and rapidly developing field in which fundamental deformation behaviours can be observed from experiments performed on comparatively small amounts of material. These methods are particularly useful when there is limited source material to facilitate a sufficient number of standard specimen tests, if any at all. Such situations include the development of new materials or when performing routine maintenance/inspection studies of in-service components, requiring that material conditions are updated with service exposure. The potentially more challenging loading conditions and complex stress states experienced by small specimens, in comparison with standard specimen geometries, has led to a tendency for these methods to be used in ranking studies rather than for fundamental material parameter determination. Classifying a specimen as "small" can be subjective, and in the present work the focus is to review testing methods that utilise specimens with characteristic dimensions of less than 50 mm. By doing this, observations made here will be relevant to industrial service monitoring problems, wherein small samples of material are extracted and tested from operational components in such a way that structural integrity is not compromised. Whilst recently the majority of small specimen test techniques development have focused on the determination of creep behaviour/properties as well as sub-size tensile testing, attention is given here to small specimen testing methods for determining specific tensile, fatigue, fracture, and crack growth properties. These areas are currently underrepresented in published reviews. The suitability of specimens and methods is discussed here, along with associated advantages and disadvantages.

Keywords Small specimen · Tensile · Fatigue · Fracture · Crack growth

J. Kazakeviciute
Faculty of Engineering, University of Nottingham, UK, NG7 2RD
E-mail: julija.kazakeviciute@nottingham.ac.uk

J. P. Rouse
Faculty of Engineering, University of Nottingham, UK, NG7 2RD
E-mail: james.rouse@nottingham.ac.uk

D. S. A. De Focatiis
Faculty of Engineering, University of Nottingham, UK, NG7 2RD
E-mail: davide.defocatiis@nottingham.ac.uk

C. J. Hyde Faculty of Engineering, University of Nottingham, UK, NG7 2RD
E-mail: christopher.hyde@nottingham.ac.uk

1 Introduction

Small specimen testing is becoming increasingly relevant in industry and new capabilities are continuously being developed for identifying a wide range of material properties. Generally, small specimens are used in situations where there is insufficient material to make full size specimens, where handling full size specimens is undesirable or when properties of a small amount of material are of interest.

There could be insufficient material to make full size specimens when a new material is being developed, as due to large costs only small amounts of material are initially made. Another reason could be that a part of an in-use component is tested, such as when a scoop sample is taken from a steam pipe. Sometimes the components, the properties of which are of interest, are too small to make a full size specimen, such as when airfoil parts of the service-exposed gas turbine blades, requiring to reduce the size of the specimen tested.

Handling full size specimens may be undesirable when irradiated material is being tested, as irradiating large amounts

of material might be difficult in test reactors, also, transporting large amounts of irradiated materials is a safety issue. Due to in-service conditions, sometimes materials need to be tested in combustible liquids, so small specimens need to be used in order to minimize the amount of liquid needed. When precise temperature control is needed, such as when testing in cryogenic temperatures, small specimens are preferable, as temperature control on a small amount of material is easier.

Properties of small components may be of particular interest when the effect of a coating is investigated, such as when fatigue performance of nitrided small gear teeth is investigated. Some processing techniques, such as spot welding, result in locally changed properties. In order to investigate them specifically small specimens have to be used. Another reason to use small specimens would be when single crystal properties are investigated, for example, when the effect of loading on the activation of slip systems is of interest. Currently small specimens are mostly used in power generation, nuclear and aerospace industries, however, they usually do not replace standard specimen testing.

An important challenge in small specimen testing is that much of it depends on correlating force-displacement measurements to stress-strain states in non-uniaxial load conditions. Correlations are often valid for only one material (equivalent gauge sections and lengths depend on small specimen stiffness rather than simply geometry), so new ones must be developed for different materials (for example, different correlations for steels and copper alloys). Generally, properties can be directly obtained from sub-size standard specimens, while all other specimens (such as small punch specimens or small ring specimens) require correlations in order to get information comparable to data from standard specimens (i.e. uniaxial equivalent results).

The main area of interest for the application of small specimen techniques has primarily been the power generation industry, whether for the development of new materials for power plants or for the inspection of remaining life in the components of existing ones. Recently the majority of the research in this field has been on creep testing, followed by fracture, then tensile properties, fatigue and lastly crack growth. As the first small specimen techniques developed were sub-size tensile testing, miniature disc bending and shear punch, they are already well characterized.

The size limit of interest for this review is under 50 mm in the largest dimension and over a few millimetres in gauge section and length dimensions. This is due to the fact that bulk material properties are of interest and when very small specimens are tested the properties of individual grains might be tested instead of bulk properties. The maximum size range was based loosely on the size of scoop samples, which are particularly used for inspection of in-service components. Standard specimens are generally too big to be made from scoop samples, (size comparison shown in Figures 1 (a) and (b)), therefore small specimens have to be used.

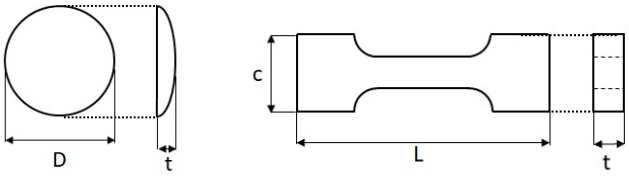

(a) (b)

Fig. 1: (a) Example of a scoop sample. *D* is around 30 mm, *t* is around 4 mm. (b) Example of a standard specimen. *L* is around 150 mm, *c* is around 20 mm and *t* is around 5 mm.

Several reviews have been written about the use of small specimens in materials testing. As the most commonly investigated small specimen application recently is creep testing, reviews on creep have been written by Dyson et al. [1] and by Hyde et al. [2]. The use of small punch specimens for creep properties has been reviewed by Rouse et al. [3]. A review on tests performed exclusively on irradiated materials in the size range of tens of nanometers to tens of micrometers has been written by Hosemann et al. [4] and a review on fatigue testing of microfabricated materials and micro-electro-mechanical systems has been written by Connolley et al. [5], they focus specifically on the small scale material behaviour, as opposed to bulk material behaviour. Small tensile specimen testing has been reviewed recently, the reviews focused on sub-size tensile specimens [6], with a view to develop a novel small tensile specimen based on sub-size specimen geometry [7] or sub-size tensile specimen testing, small punch specimen testing and the strain measurement techniques, specimen preparation and testing setup [8]. None of them have focused on what specific material properties can be acquired using specific small specimens. The most recent review of the use of small punch specimens, which compliments this review, has been written by Arunkumar [9]. The most recent reviews on the general use of small specimens was by Karthik et al. (excluding creep) [10] and Lucon (including creep) [11], not focusing on the specific material properties which have been acquired using small specimen testing techniques either. One of them describes the thoroughly researched testing techniques and the limitations which have been investigated, but not novel specimen geometries and testing techniques [11]. The other one also describes the well researched techniques, as well as the measuring techniques, specimen preparation, size effects and applications [10].

One of the challenges in the field is testing materials with a sufficient number of grains to be still representative of bulk material. If there are not enough grains in the cross-section of the specimen being tested the results will not rep-

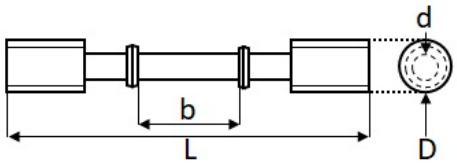

Fig. 2: Sub-size standard creep specimen. *L* is around 30 mm, *b* is around 10 mm, *d* is around 2 mm and *D* is around 10 mm.

resent a homogenized "bulk" material response, due to testing microscopic, not macroscopic material properties. This limitation is particularly evident when attempting to test a material with large grains. Due to these limitations and the complexity in interpreting test results small specimen methods have generally not received much attention from standardization organizations. It is the hope of authors that this review will increase awareness of small specimen techniques and drive wider utilization.

Another challenge is accurately evaluating the displacement, as due to specimen size and loading methods LVDTs might be inaccurate. In general, most small specimen tests use crosshead displacement (either compliance corrected or not), the accuracy of which depends significantly on the setup and the accuracy of compliance corrections, LVDT measurements or some type of non-contact displacement measurement technique, such as digital image correlation. Digital image correlation in particular enables to track inhomogeneous stress-strain behaviour. The strain measurement techniques are covered well in [8] and [6].

2 Specimen overview

Specimens generally can be classified into four different categories: sub-size standard specimens, small punch specimens, indentation specimens and bespoke specimens. These categories were chosen due to the amount of research done using those specimens and geometrical similarities they have.

As small specimens have recently been mostly used for the investigation of creep properties, it is appropriate to add small creep specimens to this overview. They will not be added to the specimen summary table due to not being the focus of this review. The specimens used for small specimen creep testing come from all subcategories. Sub-size standard creep specimens used are shown in Figure 2.

Small punch specimens used for creep testing were round, as shown in Figure 3 (a). The specimen during a small punch test (SPT) is usually loaded by clamping it between dies and pushing a semi-spherical punch through it, as shown in Figure 3 (b).

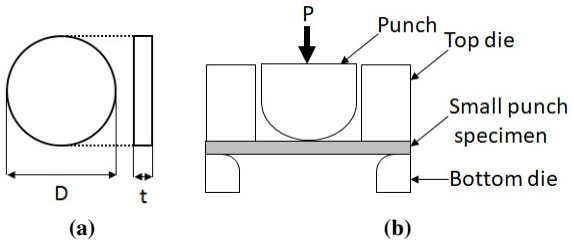

Fig. 3: (a) Small punch specimen for creep testing. *D* is around 8 mm, *t* is around 0.5 mm. (b) Small punch testing diagram.

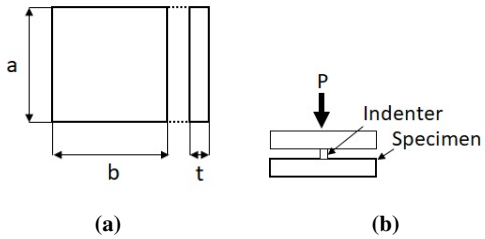

Fig. 4: (a) Indentation specimen. *a* is around 10 mm, *b* is around 10 mm and *t* is around 1 mm. (b) Indentation specimen testing diagram.

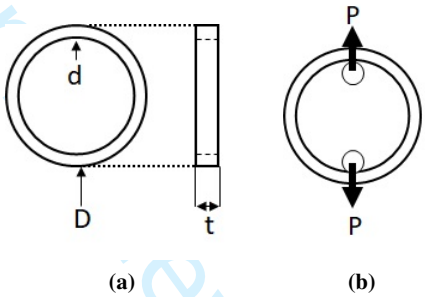

Fig. 5: (a) Small ring specimen. *D* is 11 mm, *d* is 9 mm and *t* is 2 mm. (b) Small ring specimen testing diagram.

Indentation specimens used were rectangular plates for instrumented indentation, as shown in Figure 4 (a). Indenters of a variety of geometries were used, the indenter is pushed into the specimen and the load/displacement response is recorded, as per Figure 4 (b).

Bespoke specimens include small ring specimens (Figure 5 (a), they were loaded by applying a constant load between the pins as per the loading diagram in Figure 5 (b)) and two-bar specimens shown in Figure 6 (a), also loaded by a constant load between pins, as per the diagram in Figure 6 (b). More detail about these specimens, their dimensions and testing considerations can be found in review by Dyson et al. [1] and Hyde et al. [2].

Examples from all subcategories can be found when tensile properties are of interest. Sub-size standard specimens

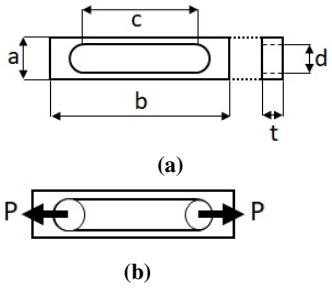

Fig. 6: (a) Two-bar specimen. *a* is around 9 mm, *b* is around 26 mm, *c* is around 13 mm, *d* is around 5 mm and *t* is around 1 mm. (b) Two-bar specimen testing diagram.

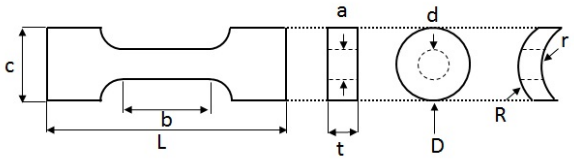

Fig. 7: Dog-bone specimen. Can be flat, round or curved. *L* varies between 2.4 mm and 37 mm, *a* varies between 0.3 mm and 4 mm, *b* varies between 0.4 mm and 22 mm, *c* varies between 1.6 mm and 10 mm, *d* varies between 2 mm and 3 mm, *t* varies between 0.15 mm and 2 mm, *D* is mentioned once and is around 6 mm and *R* is 5.44 mm with *r* equal to 4.84 mm. In some cases the thickness is not uniform [12].

include various kinds of dog-bone specimens as shown in Figure 7, button-head specimens as shown in Figure 8 (a) and round bar specimens as shown in Figure 8 (b). One sub-size standard fatigue specimen was also used, shown in Figure 8 (c).

Small punch specimens used were either round (Figure 9 (a), essentially the same as small punch specimens used for creep testing) or square (Figure 9 (b)).

One study investigated small punch specimens made from a curved tube, as shown in Figure 10 (a), which were loaded in a way shown in Figure 10 (b). Indentation specimen geometry for automated ball indentation (ABI) testing was generally not specified, which makes sense as their geometry/ dimensions do not influence the results, provided a flat surface is available and the specimen is thick enough. The minimum thickness should be either 2 to 4 times the indentation diameter or more than 10 times the indentation depth, whichever one is smaller [13].

Bespoke specimens include octagonal specimens for hydraulic bulge testing, shown in Figure 11 (a). They were loaded by clamping them between dies and applying pressurized hydraulic oil under increasing pressure until they failed, as per Figure 11 (b).

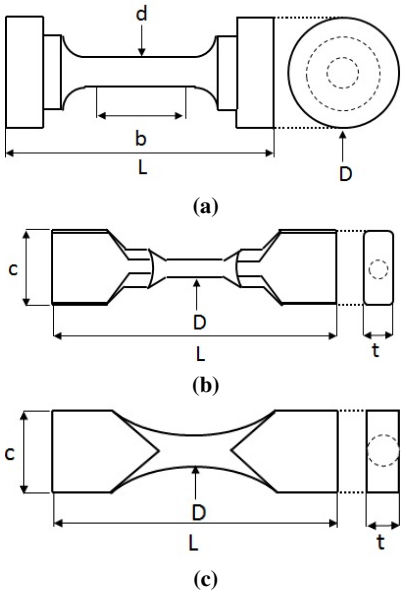

Fig. 8: (a) Button head specimen. *L* varies between 34 mm and 35 mm, *b* varies between 4 mm and 18 mm, *d* varies between 2 and 3 mm and *D* varies between 8 mm and 10 mm. (b) Round bar specimen. *L* is 24 mm, *c* is 6 mm, *D* is 1 mm and *t* is 2 mm. (c) Small hourglass specimen. *L* is 25.4 mm, *c* is 4.96 mm, *D* is 1.25 mm and *t* is 1.52 mm.

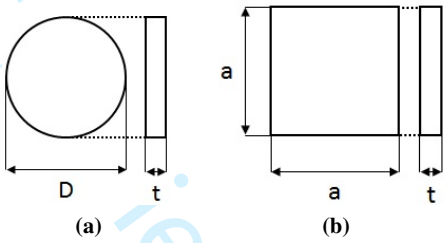

Fig. 9: (a) Round small punch specimen. *D* varies between 3 mm and 10 mm and *t* varies between 0.1 mm and 1 mm. (b) Square small punch specimen. *a* is either 5 mm or 10 mm, *t* varies between 0.25 mm and 0.7 mm.

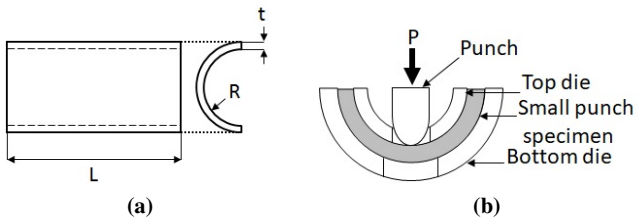

Fig. 10: (a) Curved small punch specimen. *L* is 11 mm, *R* is 2.825 mm and *t* is 0.45 mm. (b) Curved small punch specimen testing diagram.

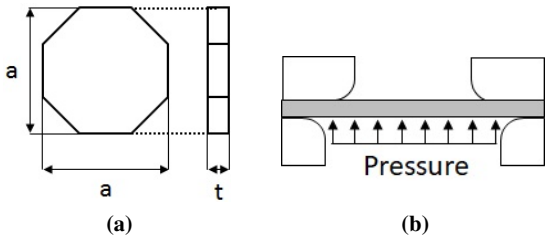

Fig. 11: (a) Octagonal hydraulic bulge specimen. *a* is 10 mm, *t* is 0.5 mm. *L* is 11 mm, *R* is 2.825 mm and *t* is 0.45 mm. (b) Hydraulic bulge test testing diagram.

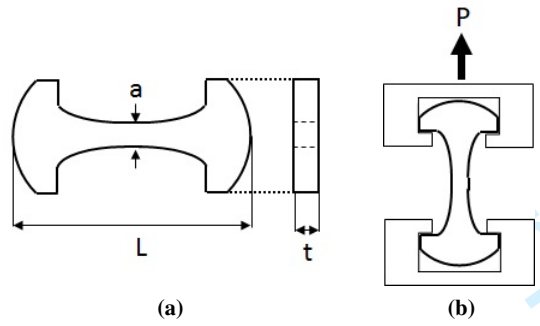

Fig. 12: (a) Miniaturized tension specimen. *L* is 3 mm, *a* is 0.5 mm and *t* is unknown. (b) Miniaturized tension specimen testing diagram.

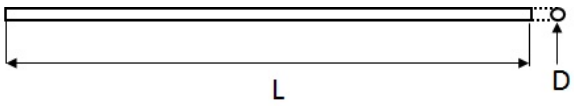

Fig. 13: Wire specimen. *L* is 20 mm and *D* is 0.1 mm.

Another geometry of specimen included were miniaturized tension specimens, shown in Figure 12 (a). They were loaded by hooking the loading arms around the flats of the specimen, as shown in Figure 12 (b).

Wire specimens shown in Figure 13 were also included. They were loaded in an unspecified way, but likely by wrapping the ends of the wire around the loading setup.

Another specimen type included was disc tensile specimens, shown in Figure 14 (a). They were tested by clamping them between two dies with a recess, to ensure full clamping, as per Figure 14 (b). A similar specimen was also used, called either the ultra small size specimen or micro tensile specimen, shown in Figure 14 (c), loaded similarly to the disc tensile specimens. A modified ultra-miniature specimen (shown in Figure 14 (d)) was also used.

The other specimens included were made from a tube in a shape of a dog-bone shown in Figure 15. The loading method was not explained. Small ring specimens of the dimensions specified earlier were also used for tensile testing.

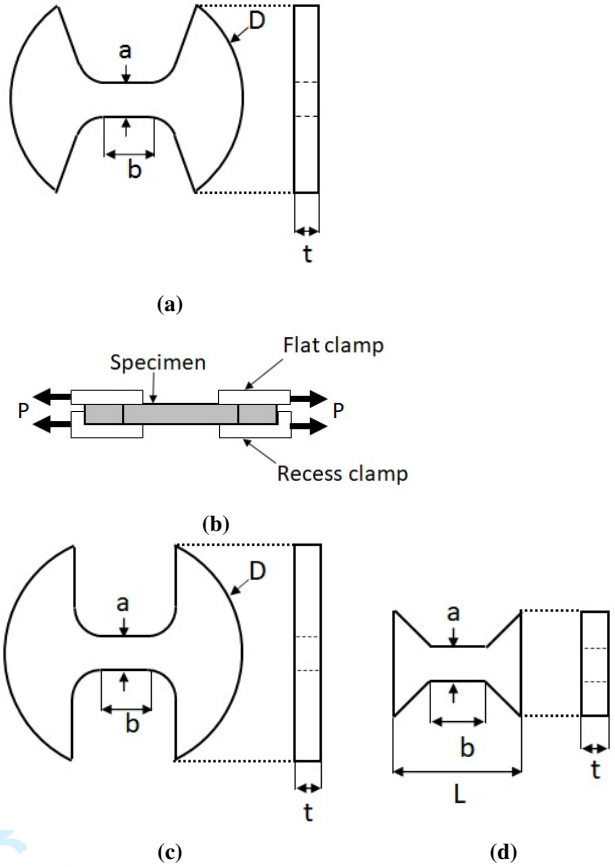

Fig. 14: (a) Disc tensile specimen. *D* is 9.44 mm, *a* is 2 mm, *b* is 2.06 mm and *t* is 0.5 mm. (b) Testing diagram of a disc tensile specimen. (c) Ultra small size specimen, also known as micro tensile specimen. *D* is 8 mm or 10 mm, *a* is 1.5 mm, *b* is 2.6 mm or 3 mm and *t* is 0.5 mm. (d) Modified ultra-miniature specimen. *L* is 5.5 mm, *a* is 0.4 mm, *b* is 2.3 mm and *t* is 0.25 mm.

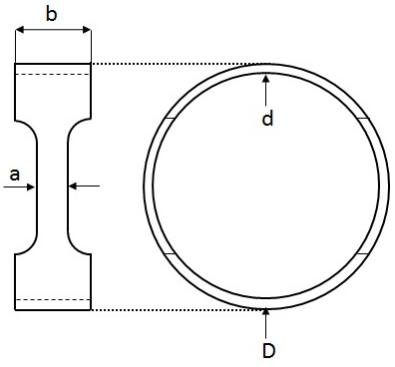

Fig. 15: Dog-bone shaped specimen cut from a tube. *a* is 1 mm, *b* is 3 mm, *d* is 9.35 mm and *D* is 10.5 mm.

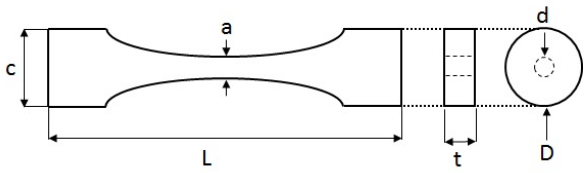

Fig. 16: Small hourglass specimen. *L* is 45 or 30 mm, *a* is 3 or 4 mm, *c* is 6 or 7 mm, *t* is 0.5 mm and *d* is either 1 mm or 2.1 mm.

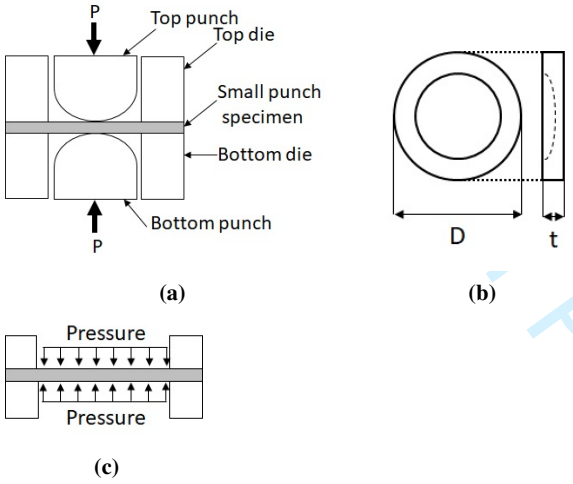

Fig. 17: (a) Small punch specimen fatigue loading diagram. (b) Hydraulic bulge fatigue specimen. *D* is 8 mm and *t* is 0.4 mm. (c) Hydraulic bulge fatigue loading diagram.

Small fatigue specimens come in all four categories as well. Sub-size standard specimens were dog-bone specimens described earlier, button-head specimens and hourglass specimens shown in Figure 16, and sub-size fatigue specimens described earlier.

Small punch specimens, loaded according to the diagram in the Figure 17 (a) were used for fatigue testing with alternating deformation applied by the top and the bottom punches. Similar to the small punch, a hydraulic bulge specimen, shown in Figure 17 (b), was loaded with alternating pressure applied on the top and the bottom side of it, as per Figure 17 (c).

ABI specimens are unspecified and bespoke specimens are small high cycle fatigue specimens shown in Figure 18 (a), modified Krouse type specimens shown in Figure 18 (b), small flat disc specimens shown in Figure 18 (c) (loaded similarly to the disc tensile specimens) and wire specimens. Small cruciform specimens (used to test material behaviour under biaxial loading) also exist, but due to their dimensions being bigger than the maximum size limit of this review they are not included.

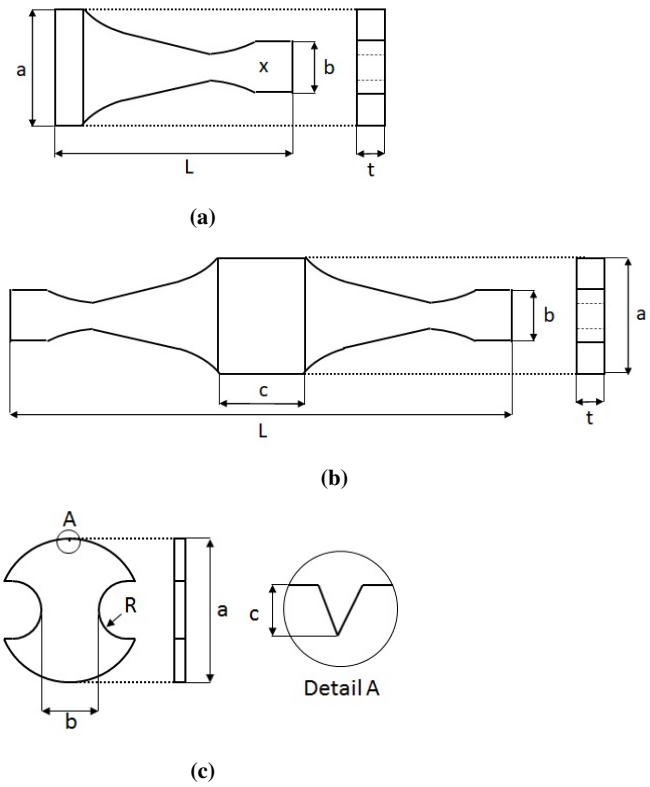

Fig. 18: (a) Specimen designed for high cycle fatigue testing. Also referred to as high cycle specimen. *L* is 13.67 mm or 15.72 mm, *a* is 6.59 mm or 6.8 mm, *b* is 4.33 mm or 3.78 mm and *t* is 1.09 mm or 1 mm, loaded by applying an oscillating load near x. (b) Modified Krouse type specimen. *L* is 30 mm, *a* is 8 mm, *b* is 4 mm, *c* is 7 mm and *t* is 0.65 mm. (c) Small flat disc specimen. *a* is 15 mm, *b* is 6 mm and *R* is 3 mm, notch at the top.

Small fracture specimens come from all of the categories. Sub-size standard specimens were sub-size compact tension (CT) specimens (square shown in Figure 19 (a), round shown in Figure 19 (b), loaded by a force applied to the pins as per Figure 19 (c)), 3-point bending specimens and sub-size Charpy specimens shown in Figure 20 (some were notched), tear toughness specimens shown in Figure 21 (loaded in the same way as compact tension specimens) and one dog-bone specimen with a cross weld.

Small punch specimens were either round or square, either notched or plain. Notches come in several types: through thickness, shown in Figure 22 (a), through length, shown in Figure 23 (they can be sharp or round) and circular shown in Figure 22 (b). The specimens with a crack through the length and a round crack were loaded with the crack facing downwards. Also, an indented small punch specimen was used, shown in Figure 22 (c), loaded with the indentation facing downwards. Small punch specimen with a notch in the mid-

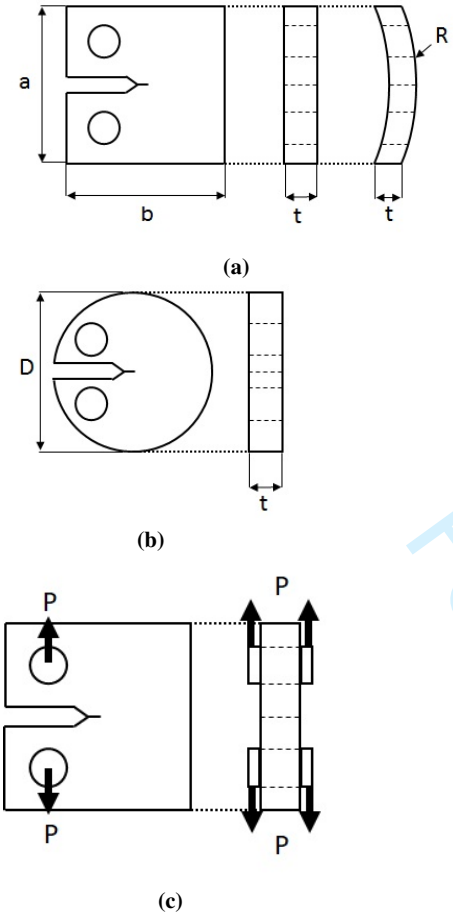

Fig. 19: (a) Compact tension specimen. Can be flat or curved. *a* and *b* vary between 10 mm and 25.4 mm, *t* is around 4 mm and *R* is 55.5 mm. (b) Round compact tension specimen. *D* is 12.5 mm and *t* is 4.03 or 4.63 mm. (c) Compact tension specimen testing diagram.

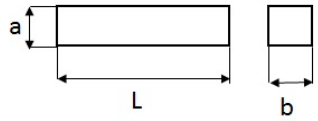

Fig. 20: 3-point bend, sub-size Charpy or mini cantilever specimen. Can be notched with notches of varied geometry. *L* varies between 16 mm and 32 mm, *a* varies between 0.5 and 5 mm and *b* varies between 1 mm and 10 mm.

dle was loaded with the notch facing upwards, unlike other notched specimens. ABI specimens were not specified.

Other specimens were a torsion test specimens shown in Figure 24 (a), loaded by applying a torque to one end as per Figure 24 (b) and a CT specimen with side grooves shown in Figure 25.

Crack propagation was investigated using sub-size standard specimens, small punch specimens and bespoke specimens. Sub-size standard specimens were dog-bone specimens with notches, curved CT specimens, mini cantilevers and wedge opening load specimens, shown in Figure 26 (a), loaded by turning a threaded rod in order to open the crack, as per Figure 26 (b). Small punch specimens were square and with a crack through length.

Regarding bespoke specimens, high cycle fatigue specimens, small fatigue specimens shown in Figure 27 (a) and C-shaped inside edge-notched (CIET) specimens shown in Figure 27 (b), loaded according to Figure 27 (c), were used. An overall summary of material properties and specimens used to get them can be seen in Table 1.

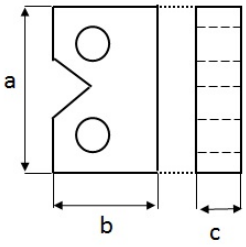

Fig. 21: Tear toughness specimen. *a* is 32 mm, *b* is 20 mm and *c* varies between 2 mm and 7 mm.

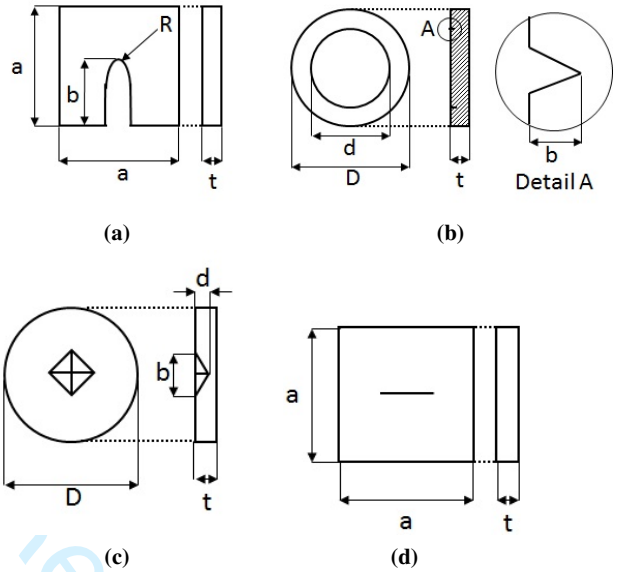

Fig. 22: (a) Small punch specimen with a notch thought thickness. *a* is 10 mm, *b* varies between 4 mm and 6 mm, *R* is around 0.1 mm and *t* is 0.5 mm. (b) Small punch specimen with a round notch. *D* is 8 mm, *d* is 2.5 mm, *b* is 0.5 mm, and *t* is 1 mm. (c) Indented small punch specimen. *D* is 3 mm, *b* and *d* depend on the indenter used and the force applied and *t* varies between 0.286 mm and 0.344 mm. (d) Small punch specimen with a notch in the middle. *a* is 10 mm, *t* is 0.5 mm and the notch is about 1 mm long.

Table 1: Summary of specimens and material properties acquired from testing them. T is tensile, F is fatigue, Fr is fracture and C is crack growth.

Specimens	Fig.	T	F	Fr	C	References
Small punch specimen						
Standard	9 (a), (b)	+	+	+	+	[14–85]
Notch through length	23 (a), (b)			+	+	[86–93]
Notch through thickness	22 (a)			+		[94, 39, 95, 96]
Indented	22 (c)			+		[97]
Circular notch	22 (b)			+		[98]
Curved	10 (a)	+				[69]
Middle notch	22 (d)			+		[99]
ABI		+	+	+		[20, 100, 101, 49, 61, 102–119]
Dog-bone specimen						
Standard	7	+	+	+	+	[120–129, 72, 130, 77, 131–133, 12, 134]
Curved	7	+				[135]
Tube	15 (a)	+				[135]
3-point bend, Charpy, mini cantilever	20			+	+	[136–140, 51, 141–150]
Hourglass specimen	8 (c), 17 (a)	+	+		+	[151, 152, 126, 153–158, 134, 80]
CT specimen						
Standard	19 (a)			+		[159–163, 73, 164–168]
Curved	19 (a)				+	[169]
Notched	25			+		[170]
Round bar specimen	8 (b)	+	+			[171, 172, 155–157]
High cycle fatigue specimen	18 (a)		+			[173–175]
Button-head specimen	8 (a)	+	+		+	[176, 125]
Micro tensile specimen	14 (c)	+				[7, 177]
Small fatigue specimen	27 (b)		+		+	[178, 129]
Torsion test specimen	24 (a)			+		[179, 180]
CIET specimen	27 (b)				+	[181]
Disc tensile specimen	14 (a)	+				[182]
Hydraulic bulge fatigue specimen	9 (a)		+		+	[183]
Hydraulic bulge specimen	11 (a)	+				[184]
Miniaturized tensile specimen	12 (a)	+				[185]
Modified Krouse specimen	18 (b)		+			[186]
Modified ultra-miniature specimen	14 (d)	+				[187]
Small flat disc specimen	17 (b)		+			[188]
Small ring specimen	5 (a)	+				[189]
Tear toughness specimen	21			+		[190]
Wedge opening load specimen	26 (a)				+	[191]
Wire specimen	13 (a)	+	+			[192]

3 Standardisation of small specimen testing

Small punch specimen testing is in progress of being standardized. A pre-normative document was created in 2007, entitled "Small Punch Test Method for Metallic Materials" [193]. The ASTM standard for small punch testing of metallic material was published in 2020 [194]. A European standard is also being developed, primarily based on the pre-normative document. Currently a draft version for public comment is available [195]. There are national standards for small punch testing in China (tensile properties at room temperature) [196, 197] and Japan (small punch creep test for residual life) [198]. Two sub-size Charpy specimen geometries are a part of the ASTM E2248 [199] (a=3 mm, b=4 mm, L=27 mm and a=b=4.83 mm, L=26.565 mm).

There are several standards for indentation testing [200–202], however, none of them are applicable to the ABI testing discussed in this review. They all describe a methodology of how to find a variety of hardness values, and indentation material properties as opposed to tensile, fatigue, fracture toughness or crack growth properties. Automated ball indentation, which is applicable to this review, is used to get material properties equivalent to uniaxial and does not have associated standards.

All other specimens discussed in this review are not standard. Some of them are sub-size standard specimens, however these fall outside the scope of relevant standards documents, due to their size. Others are based on standard specimens but are modified in order to acquire more represen-

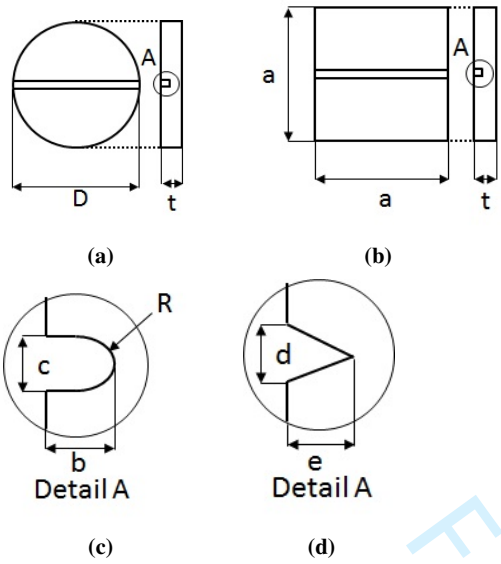

Fig. 23: Small punch specimen with a notch through length. Can be round (a) or square (b), notches can be round (c) or sharp (d). *D* varies between 8 mm and 10 mm, *a* varies between 10 mm and 20 mm, *b* is around 0.15 mm, *c* is 0.278 mm, *d* is around 0.2 mm, *e* varies between 0.2 and 0.5 mm and *R* is around 0.1 mm.

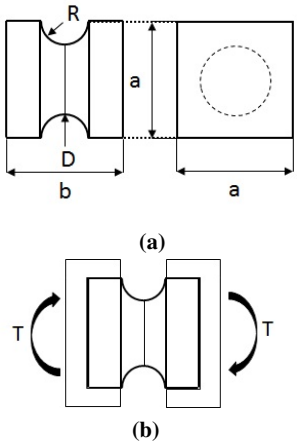

Fig. 24: (a) Specimen for testing the strength of hot isostatic press (HIP) joints. Also referred to as torsion test specimen. *a* is 6 mm, *b* is 6 mm, *D* is 1.8 mm and *R* is 1.2 mm. (b) Torsion test specimen loading diagram.

tative results, such as changing the specimen thickness not proportionally to the reduction in size.

In order for a testing technique to be standardized a testing method has to be clearly described and the results have to be repeatable, which is achieved by a round robin experiment, where tests using the technique are performed in several different laboratories. Round robin experiments have been performed for various specimens, including small punch

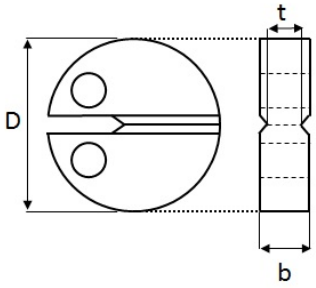

Fig. 25: Round compact tension specimen with side notches. *D* is 26 mm, *b* is 10 mm and *t* was varied between 4 mm and 9.5 mm.

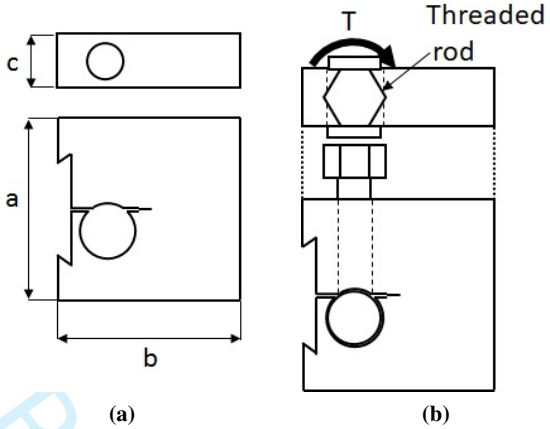

Fig. 26: (a) Wedge opening load specimen. *a* is 15.75 mm, *b* is 20.25 mm and *c* is 6.35 mm. (b) Wedge opening load specimen testing diagram.

(for determining yield strength, ultimate tensile strength, fracture toughness and fracture appearance transition temperature), ABI (for determining yield strength, hardening behaviour and ultimate tensile strength from it) and CT (for determining fracture toughness using the Master Curve method).

It is also beneficial to characterize the testing techniques in terms of the effects of setup parameters, what materials it can be used to test and what microstructural limitations apply. The level of scatter between repeated tests is also important to evaluate, as large values of scatter could hide small differences in test results caused by other factors, and finding a test result out of that range could mean it is not valid due to errors during setup. Ideally the scatter in the test results from small specimen test results should be equal or less than the scatter of the standard technique for finding equivalent material properties, however, it is usually higher due to microstructure effects and a lack of standardized testing and data interpretation procedures.

Due to the fact that the data interpretation methods for small specimens are not as straightforward as for standard

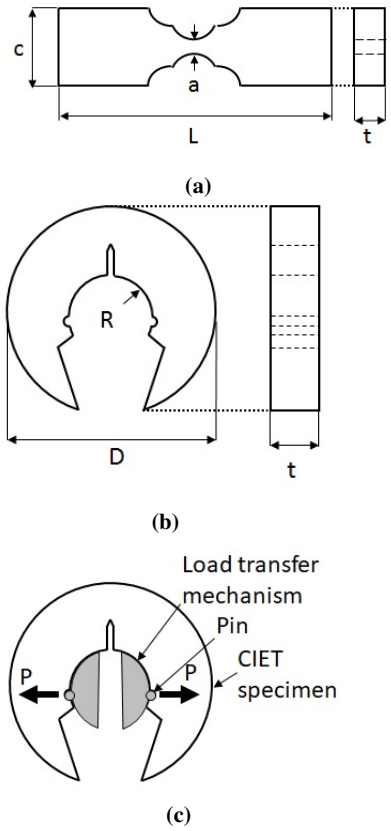

Fig. 27: (a) Small fatigue specimen. L is 26 mm or 2.4 mm, a is 1 mm or 0.3 mm, c is 4 mm or 1.8 mm and t is 1 mm or 0.3 mm. (b) C-shaped inside edge-notched tension (CIET) specimen. D varies between 20 mm and 60 mm, R is 6 mm and t varies between 5 mm and 15 mm. (c) CIET specimen testing diagram.

specimens, both experimental technique and data interpretation methods can introduce uncertainties into the final results and both sources of uncertainty should be investigated, which is discussed in more detail in [10].

In general the accuracy of the small specimen technique is validated by performing a small specimen test, evaluating the material properties of interest, then comparing them to the properties acquired from standard testing. These can be either acquired as a supplement of the small specimen test, if the comparison of the exact material is of interest, or from a material database, such as MatWeb, MATDAT and a large number of others. In some cases validation cannot be performed due to a lack of material to make standard specimens of equivalent properties. In those cases small specimens can either be used for ranking or an interpretation method which has been proven to work for a similar material can be used.

Table 2: Materials and specimens from which Young's modulus was acquired.

	Steels	Aluminium alloys	Nickel alloys
Sub-size standard specimens	[129, 120, 140, 131, 80]	[121]	[124, 125]
Small punch specimens	[66, 46]	[66]	
Bespoke specimens	[182, 135]	[189]	

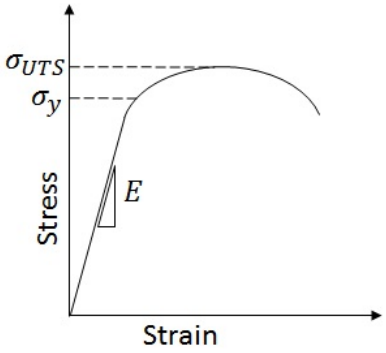

Fig. 28: Example stress-strain curve. E is Young's modulus, σ_y is yield stress, σ_{UTS} is ultimate tensile strength.

4 Tensile testing

4.1 Young's modulus

Small specimen testing of Young's modulus was done on a wide range of materials and specimens, shown in Table 2. The bespoke specimens used were disc tensile specimens (Figure 14 (a)), specimens made from a tube in the shape of a dog-bone (Figure 15) and small ring specimens. When sub-size standard specimens were tested Young's modulus was determined directly from stress-strain curves and matched the results from standard uniaxial testing well when verified against standard uniaxial test results [124, 125, 131, 80]. An example stress-strain curve is shown in Figure 28.

The SPT results are not as straightforward to interpret. In the example test results shown in Figure 29 the force-displacement curve is divided into five regions. The slope parameter of region I was found to relate to Young's modulus for aluminium alloys [66].

Husain [46] developed an inverse finite element analysis (FEA) method which evaluated Young's modulus between 17% lower and 11% higher than the results from testing standard specimens, which is promising. The disc tensile specimen worked rather well, apart from finding about 6% lower values for Young's modulus in comparison with uniaxial testing results, likely due to inelastic effects and micro-plasticity below proportional limit [182]. The elastic

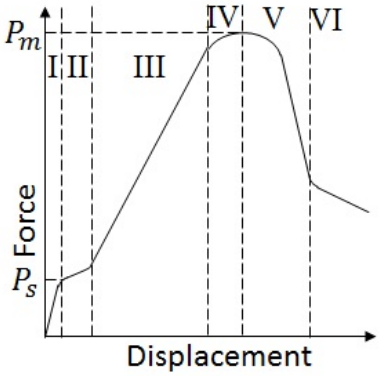

Fig. 29: Example force-displacement curve from small punch testing. P_s is limit load, P_m is maximum load. Region I represents elastic bending, region II represents plastic bending, region III represents membrane-like behaviour due to the balance of work hardening and stretching, region IV is when necking and crack initiation happens, region V has fracture softening behaviour and region VI is when final fracture occurs.

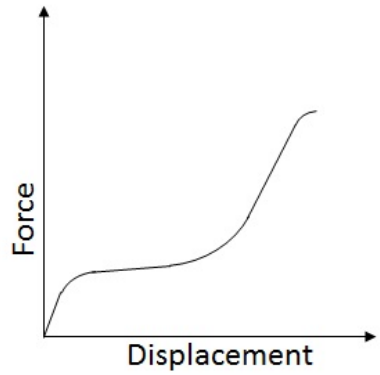

Fig. 30: Example force-displacement curve from small ring testing.

part of the stress-strain curve can be calculated from small ring specimen force-displacement curve, the results agree with standard testing results well, however there currently is no method to calculate Young's modulus for an unknown material [189]. The example force-displacement curve from small ring specimen testing is shown in Figure 30.

Results from all these studies suggest that Young's modulus can only be accurately determined from sub-size standard specimens (within 1.4 %), small ring specimens are promising, disc tensile specimens are good for an approximate estimate and SPT does not seem to be appropriate at all, however investigating more materials could prove otherwise.

In most cases when small specimen use is required, Young's modulus is not an important material property to evaluate, which reduces the interest in evaluating it using small specimens. For alloys based on the same metal the Young's modulus is largely independent of microsctruture, processing or heat treatment, so the main use of small specimens for evaluating it would be when new materials are being developed.

4.2 Yield strength

Small specimen testing of yield strength was performed on a wide variety of materials and specimens, shown in Table 3. The bespoke specimens used were an octagonal specimen for hydraulic bulge testing (Figure 11 (a)), miniaturized tensile specimen (Figure 12 (a)), disc tensile specimen (Figure 14 (a)), micro tensile specimen (Figure 14 (c)), modified ultra-miniature specimen (Figure 14 (d)) and a wire specimen (Figure 13).

When sub-size standard specimens were tested yield strength was determined from stress-strain curves directly [124, 125, 131, 12, 80, 134] like when standard specimens were tested; consequently it matched well with yield strength from standard specimen tensile testing results. Several authors pointed out aspects which could influence the measurement of yield strength: there needed to be enough material in the gauge section to prevent brittle failure [127], microstructure and grain size needed to be taken into account [70] and surface roughness had a significant effect of reducing the effective gauge section [126]. Roughness was particularly relevant for smaller specimens as the surface layer was a larger part of the total cross-section, therefore it needed to be accounted for if the specimens were not polished. Ge [40] found that yield stress from small specimens was higher than standard, possibly because the specimen was not optimized like others were, just reduced in size. Good agreement was seen between sub-size standard specimen tensile test results and indirect yield strength measurements based on hardness correlations for welds and heat affected zone (HAZ) [120]. Yield strength determined from varied thickness (parameter t in Figure 7) sub-size standard specimen testing results is not affected by the variable thickness [12]. Vandermeulen found that the manufacturing method is more important when making small specimens than when making standard specimens, as turning a specimen creates a cold worked layer which then increases the yield strength in comparison to reference [132].

SPT specimens could not be used to determine yield strength directly as they only produce a force-displacement curve as opposed to a stress-strain curve. Therefore various correlations based on limit load (P_s in Figure 29) were used, with different ones being applicable to different materials [66, 35, 32, 21]. In general the results after applying the correlations matched standard testing results well, apart from when the material did not exhibit a limit load [50], sometimes the results were too scattered to be used for anything

Table 3: Materials and specimens from which yield strength was acquired.

	Steels	Aluminium alloys	Nickel alloys	Titanium alloys	Copper alloys	Tungsten alloys	Magnesium alloys	Zirconium alloys
Sub-size standard specimens	[129, 135, 72, 40, 23, 120, 140, 203, 204, 202, 127, 131, 12, 80]	[122, 121]	[124–126, 132]		[126, 134]	[126, 122]		
Small punch specimens	[72, 39, 91, 23, 34, 70, 60, 37, 50, 47, 46, 63, 35, 49, 21, 65, 20, 78, 79, 85]	[60, 66, 37, 32]	[33]	[60]			[22]	[114]
ABI specimens	[205, 100, 49, 20, 64, 63, 102–105, 113, 115–119]	[109, 111, 112]		[108, 110]				[114]
Bespoke specimens	[184, 185, 182, 177, 187, 7]	[177, 7]	[177]	[177]	[7]			

other than ranking [33] or when the thickness to grain size ratio was too low (less than 19), making the results not representative of bulk material [70]. Thickness has a significant effect, especially for thinner specimens, therefore additional corrections should be used [79]. Inverse FEA could be used to acquire yield strength and could achieve good agreement with standard test results [46]. An analytical solution based on classical plate theory could also be used. It relies on a correlation between 0.2% proof stress and small punch maximum bend strength, which depends on the dimensions of the setup, limit load and the displacement to limit load, the results are within 5% of standard [58]. An attempt was made to develop a material independent correlation for power plant steels, it resulted in a wider scatter than material specific correlations [85].

One of the other specimens and testing methods used to identify yield stress was hydraulic bulge test. An example force-displacement curve is shown in Figure 31 (a). The yield stress was calculated using a correlation between limit load (P_{lim} in Figure 31 (a)) from the force-displacement curve and yield strength from standard testing and achieved good agreement with standard test results [184]. Shear punch was another testing method used, illustrated by Figure 31 (b), it was also similar to SPT, but instead of a ball the punch was flat, there was a clearance of 0.02 mm between the punch (diameter 3 mm) and the die to ensure shear deformation, and both top and bottom dies had the same diameter. An example force-displacement curve is shown in Figure 31 (c). The yield strength was calculated using a correlation between the limit load (P_γ in Figure 31 (c)) and yield strength, good agreement with standard testing results was also achieved [64, 63, 49]. Varying the thickness was found to have an effect, however it is negligible between 0.29 mm and 0.4 mm for a punch diameter of 1 mm [78]. Correlations were used to find yield strength from miniaturized tensile specimen test results [185], while inverse FEA was used to find it from the disc tensile specimen test results [182]. The use of correlations resulted in good agreement with standard testing results and inverse FEA results were within 2% of standard testing results. Inverse FEA used the estimate of the proportional limit and calculated true stress-strain behaviour to determine the yield stress.

ABI (illustrated in Figure 32, the indenter is repeatedly pushed into the material, then partially unloaded, then reloaded) also relied on correlations and had good agreement with standard testing results (within 0.5 %), even better then SPT tests when compared directly [20]. It was also used to characterize the variation of yield stress across welds [102–105], the effect of high pressure torsion processing [112], the effect of machining [117] due to being able to evaluate material properties locally. The effects of temperature [108], loading rate [110], effect of heat treatment [111, 113] and test setup parameters [118] were successfully investigated, good agreement was found with standard specimen test results. Alternative methods for calculating yield stress were investigated as well, such as neural networks [110], which result in better agreement between ABI and standard results than constitutive behaviour based correlations, and inverse analysis, which is shown to be a promising technique [115].

Micro tensile specimen test results agree well with standard test results [7], in particular when video gauge, as opposed to a mechanical extensometer is used [177]. Modified ultra-miniature specimen underestimates yield stress in comparison to sub-size standard specimens [7].

The wire specimen was an interesting case, as the yield strength was identified from a stress-strain curve, and it was significantly higher than of standard specimens, due to size effects [192]. Size effect in this case is the increase of material strength when small structures or small volumes of material are tested. In this case it is likely that the size effect was caused by a combination of both factors, as the microstructure is not specified.

The effect of composition could be identified using sub-size standard specimens [203, 204]. For pressed and sintered material yield strength calculated from SPT results was very similar to calculated ultimate tensile strength (UTS) due to the brittleness of the material [34].

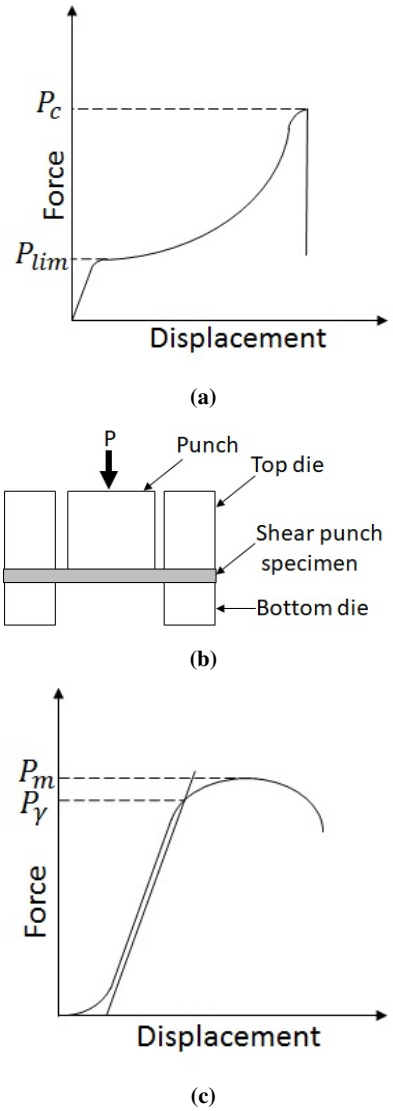

Fig. 31: (a) Example pressure-displacement curve from hydraulic bulge test. P_{lim} is limit load, P_c is critical load. (b) Example force-displacement curve from shear punch test. P_γ is limit load, P_m is maximum load. (c) Shear punch testing diagram.

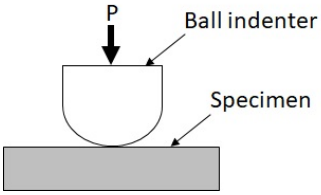

Fig. 32: ABI loading diagram.

Overall, sub-size standard specimens seem to be the most suitable for yield strength, provided the geometry is appropriate, achieving exactly the same yield strength as standard specimens in some cases. In other cases the yield strength evaluated can be up to 10 % different from standard. SPT is suitable in a lot of cases, but different correlations apply for different materials and sometimes it cannot be used. Shear punch and hydraulic bulge tests are similar to SPT as they both rely on correlations and the results agree with standard results well, however more studies should be done to investigate potential issues. ABI is a thoroughly investigated technique, suitable for a variety of materials and resulting in good agreement between standard and ABI test results. In order to further the applicability of small specimens for determining yield strength more detailed investigations into the bespoke specimens used should be done, as there has been a lot of interest and research into sub-size standard tensile specimens, small punch specimens and ABI. All testing techniques described here would also benefit from repeatability investigations.

4.3 UTS

Small specimen testing of UTS was performed on a wide variety of materials and specimens, shown in Table 4. The bespoke specimens were octagonal hydraulic bulge specimens (Figure 11 (a)), disc tensile specimen (Figure 14 (a)), miniaturized tensile specimens (Figure 12 (a)), micro tensile specimens (Figure 14 (c)), modified ultra-miniature specimens (Figure 14 (d)) and wire specimens (Figure 13).

If sub-size standard specimens were used UTS could be determined directly from stress-strain curves, as per Figure 28. The gauge section needed have enough material to resist necking and not fail before UTS equivalent to UTS from standard specimen testing was reached [127]. For brittle materials the misalignment when manufacturing and loading could lead to significant differences between UTS acquired from small and standard specimens [122]. Surface roughness needed to be accounted for by subtracting the roughness from the specimen width and thickness to calculate the effective load-bearing cross-section, as that resulted in better agreement with standard testing results [126]. Similarly to yield strength, UTS is increased by cold working the surface when manufacturing the specimen, making it not representative of bulk material properties [132]. One of the sub-size standard specimen testing techniques relied on correlations instead of direct evaluation, in order to take the necking zone into account. It produced better results than without using the correlation [52]. The size effect was investigated for a sub-size hourglass specimen, it was discovered that UTS is mostly independent of specimen dimensions [158]. UTS is also mostly independent of varied thickness (parameter t in Figure 7) in sub-size standard specimens [12].

Table 4: Materials and specimens from which UTS was acquired.

	Steels	Aluminium alloys	Nickel alloys	Titanium alloys	Copper alloys	Tungsten alloys	Magnesium alloys	Zirconium alloys
Sub-size standard specimens	[127, 129, 135, 72, 40, 23, 120, 140, 203, 204, 122, 52, 154, 131, 158, 12, 80]	[122, 121]	[124–126, 132]		[126, 134]	[126, 122]		
Small punch specimens	[60, 72, 39, 91, 23, 34, 70, 37, 50, 47, 59, 46, 49, 63, 35, 21, 65, 20, 78, 79]	[60, 66, 37, 32]	[33]	[60]			[22]	[114]
ABI specimens	[205, 100, 49, 101, 20, 64, 63, 102–105, 113, 117–119]	[109, 111, 112]		[108]				[114]
Bespoke specimens	[184, 185, 182, 192, 177, 187, 7]	[177, 7]	[177]	[177]	[7]		[15]	

Determining UTS from SPT specimen results relied on correlations between UTS and maximum load (P_m in Figure 28), and, much like for yield strength, they were also material specific. Generally the results after applying the correlation agreed with the results from standard specimen testing well, but scatter was bigger than when standard specimens were used [72], sometimes making it impossible to use SPT as anything other than a ranking tool [33]. When developing a new correlation minimizing the scatter is important as scatter bands that are too wide make it difficult if not impossible to determine material properties [90]. The results from thinner specimens require additional corrections to be representative of bulk material [79]. If full size specimens were manufactured in a way that resulted in anisotropy between outer surface and the center of the specimen, testing SPT specimens cut as slices from the gauge section of the standard specimens did not result in the same material properties as standard specimens [22]. When a standard specimen is tested the difference in material properties is averaged out, but when a SPT specimen is tested only the central region is actually tested.

Bespoke specimens and testing methods included hydraulic bulge [184] (example result shown in Figure 31 (a)) and shear punch (example result shown in Figure 31 (c)) [64, 63, 49], both of which relied on correlations based on the critical or maximum load and had good agreement with standard tests. The thickness of the shear punch specimen has a significant effect on the results, but not when the thickness is between 0.29 and 0.4 mm [78]. Shear punch jump test, producing similar data to tensile jump test, also resulted in good agreement between calculated UTS and uniaxial UTS [15]. The more unusual specimens were the miniaturized tensile specimens and disc tensile specimens, one of which relied on correlations [185] and the other on inverse FEA [182]. ABI was also used, with a series of calculations applied in order to calculate UTS and it achieved reasonably good agreement with uniaxial results [20, 101, 49]. Similarly to yield stress, UTS was also evaluated across welds using ABI, due to its ability to measure material properties locally [102–105]. Similarly to determining yield stress, the effects of various parameters were investigated for determining UTS from ABI test results.

Micro tensile specimen test results agree well with standard test results [7], in particular when video gauge, as opposed to a mechanical extensometer is used [177]. Modified ultra-miniature specimen underestimates UTS in comparison to sub-size standard specimens [7].

Wire specimens were not very good for representing bulk properties, as UTS was much higher than from standard specimens, due to size effects, however, bulk material properties were not of interest in this particular application [192].

Other observations regarding identifying UTS using small specimens were that small curved dog-bone specimens in combination with tube cut in the shape of a dog-bone can also identify anisotropy in steel tubes [135] and that for SPT there was a critical thickness to grain size ratio (25) over which correlations between maximum load and UTS applied [70].

Overall UTS can be identified from both sub-size standard (within 10 %, similar to standard test scatter) and SPT specimens, however the results from SPT are less reliable and immediately usable as a suitable correlation needs to be identified or developed. ABI is also suitable for determining UTS, with good agreement to standard test results, within 2 % to 15 % of standard results. Similarly to yield stress, UTS evaluation from small specimen test results would benefit from further investigations into the bespoke specimens used, as well as thorough investigations of repeatability.

4.4 Plastic behaviour

Plastic behaviour is the shape of the uniaxial stress-strain curve beyond the yield stress. Materials and specimens from which plastic behaviour was investigated using small specimens are shown in Table 5. Disc tensile specimens (Figure

Table 5: Materials and specimens from which plastic behaviour was acquired.

	Steels	Aluminium alloys	Titanium alloys	Zirconium alloys
Sub-size standard specimens	[127, 129, 140]	[121]		
Small punch specimens	[46, 63, 16, 17, 54]			[114]
ABI specimens	[100, 101, 63, 102–105, 113, 115–119]	[109, 112]	[108, 110]	[114]
Bespoke specimens	[182]	[189]		

Table 6: Materials and specimens from which fracture strain and/or ductility parameters were acquired.

	Steels	Magnesium alloys
Sub-size standard specimens	[40, 171]	
Small punch specimens	[39]	[22]

14 (a)) and small ring specimens were the bespoke specimens used.

The objective here was to obtain the full stress-strain curve and subsequently parameters for plasticity models. Generally plastic behaviour was directly evaluated from stress-strain curves, especially in the case of sub-size standard specimens. In one case the stress-strain response of a small tensile specimen was significantly different from standard specimen testing results [40], thus showing that even when sub-size standard specimens are used the results might not necessarily agree with standard results. ABI is suitable for finding coefficients of a power law hardening material model, by calculating a stress-strain curve from the indentation diameter, the indenter diameter, applied load and a correlation parameter, which is found iteratively. The strain hardening exponent can be found to within 2% of the actual value [101]. There was a linear correlation between small punch strain hardening index (calculated from maximum load and limit load) and tensile test strain hardening index, which allowed to convert one into another. Shear punch method used a similar correlation between the shear punch hardening coefficient and the tensile hardening coefficient. Due to larger scatter, it was less accurate than small punch testing [63]. Inverse FEA was used as well, in both cases the results matched uniaxial tests well, at least up to UTS, then diverged due to necking [182, 46]. It also had a potential issue regarding the uniqueness of the solution as different stress-strain curves could potentially result in the same small punch response. The plastic behaviour can be calculated from small ring specimen testing results with good agreement to standard testing results [189].

Neural networks were used for identifying plastic behaviour from SPT data after having been trained with FEA simulations, with good results [16, 17]. As the model is sensitive to stress triaxiality, at least two experiments at different triaxialities need to be done. Also split Hopkinson bar testing setup with a small tensile specimen was developed and used successfully [121]. Much like for other tensile properties, an appropriate amount of material in the gauge section was important to get data representative of bulk material [127].

Overall, it seems that plastic behaviour can be determined well using all small specimens, at least up to UTS. Necking, occurring after UTS, is very geometry dependent, causing difficulty in calculating standard-equivalent behaviour from test results acquired by using a different geometry.

4.5 Fracture strain/Ductility

Ductility was evaluated for materials and specimens shown in Table 6. Both specimen types were only suitable for ranking. Ductility directly depends on the dimensions of the specimen, as they are reduced, so is ductility [40]. The effect of stress triaxiality on ductility was investigated using small specimens. It was discovered that for both sub-size notched specimens and standard specimens more stress triaxiality lead to fracture at lower strain [171].

4.6 Small punch load line behaviour

Research was conducted to investigate what influences small punch force-displacement results, without trying to correlate that to specific standard test results. This was done exclusively for steels, with varied SPT specimen dimensions [48, 68, 185, 53, 71, 59, 30, 82, 81]. The results showed that the yield load (P_s in Figure 29) did not depend on punch diameter, but varied as a square of sample thickness. Maximum load (P_m) increased with sample thickness [53] and punch diameter. Lower sample thickness and smaller punch diameter lead to more scatter [48].

Other observations were that the clamping force used to clamp the small punch specimen between the dies had a significant effect on the maximum load measured during SPT. Increasing the clamping force increases the maximum load measured, therefore an appropriate clamping force needs to be chosen to get material properties representative of bulk material [68]. Increasing cold work increased maximum force [185], which was also as expected, however maximum displacement did not depend on cold work. Orientation was

found to be very significant, so if the material is anisotropic it should be tested in the appropriate direction [53]. Maximum force was observed to depend on deflection rate, which agreed well with standard testing results, when numerically the same deflection rate (in mms^{-1}) and strain rate (in s^{-1}) were considered [59].

As heat treatment affects material properties, it also affects the results from small punch testing [71]. In the study where the response was compared to standard test results, good agreement was found [68]. The suitability of small punch specimen testing for evaluating thermal ageing embrittlement was investigated, however whether the results could be used as anything more than a ranking tool remains to be seen [30]. Liquid metal embrittlement was also investigated using small punch specimens without comparing the results to full-size specimens [76]. The effect of phase transformation due to deformation and loading rates was investigated, it was found that at room temperature the phase transformation enhances material performance [81]. At dynamic loading rates the heating caused by the deformation can cause thermal softening and therefore negative rate sensitivity.

4.7 Other tensile properties

Elongation at maximum load was evaluated for two magnesium alloys using SPT data and a correlation between elongation under maximum load and displacement under maximum load was found, however the success of this test depended on microstructure of the material being tested [22].

Tensile elongation was also evaluated using SPT data for a sintered material, good agreement with uniaxial results was achived [34], however trying to evaluate it for a variety of unsintered steels via a correlation between it and displacement under maximum load was not successful [37]. It could be that SPT is only suitable for determining tensile elongation for brittle materials or perhaps different correlations are needed.

Another investigation related to small punch testing was testing a piece of tube and comparing the response to a response from a flat SPT [69]. It was discovered that friction had a significant effect according to FEA and experimentally and the difference in force-displacement behaviour was due to geometry. Another investigation confirmed the effect of friction on small punch results and investigated the effect of friction on automated ball indentation test results [62]. One study found that surface finish does not have a significant effect on the results experimentally, which appears to disagree with other studies, which state that surface roughness and the coefficient of friction have a significant effect. The results of this study are likely material specific and are only valid for the range of surface roughness investigated [82].

Sub-size standard specimens were also used for identifying other tensile properties. Uniform elongation was investigated, it was discovered that it was approximately the same for both standard and sub-size specimens, however total elongation was lower than for a standard specimen [40], which is as expected due to lower gauge volume being able to deform less before failing. Varied thickness (parameter t in Figure 7) and gauge length in sub-size standard specimens affects the uniform and total elongation non-linearly [12]. There was also a successful attempt to improve the calculation for UTS by identifying the necking zone using FEA [52]. Reduction in area is similar to standard specimens, however, that depends on specimen shape and size [132, 158].

For micro tensile specimen uniform elongation was found to be within 5-10 % of standard specimens, while for modified ultra-miniature specimen both uniform and total elongation were significantly lower than for standard specimens.

Other tests that were done were small punch jump test, which was capable of producing curves similar in shape to tensile jump test, making it suitable for evaluating deformation mechanisms and evaluating strain rate sensitivity [15]. Shear punch and ABI tests were used to find uniform elongation and a good linear correlation between it and strain hardening coefficient was found [49].

5 Fatigue testing

5.1 Low cycle fatigue life

Sub-size standard specimens have been used to determine low cycle fatigue life for steels [155, 157, 206, 172] and nickel alloys [124, 125]. All tests were done with fully reversible loading.

In general small specimen test results match standard specimen results well. Round bar specimens (Figure 8 (b)) were not sensitive to size effects, while hourglass specimens (Figure 8 (c)) were [157, 155]. Surface roughness was an important factor to control for [206], however useful recommendations are lacking in the literature. Overall small specimens seem to be suitable for determining low cycle fatigue life, however size effect needs to be considered when interpreting the results. It would be beneficial to further investigate the repeatability, as well as the applicability of these tests to other materials and the limitations of the microstructure being tested.

5.2 High cycle fatigue life

High cycle fatigue testing of small specimens was investigated for an aluminium alloy using a specially designed high cycle specimen (Figure 18 (a)) [173, 174], and for a steel

using a sub-size hourglass specimen [80]. Tests were done with fully reversible loading.

The conclusions from both papers about the high cycle specimens were that microstructure had a significant influence on fatigue life as small grains without dislocations resulted in higher fatigue life. The fatigue life identified could only be used for ranking due to being lower than textbook values [173, 174]. It may be the case that grain size relative to the specimen size should be considered in order to get data that is suitable for more than ranking. Sub-size hourglass is particularly suitable for determining high cycle fatigue life, the results being within the scatter band of standard testing results [80].

For further development of small specimen high cycle fatigue life testing, it would be beneficial to test more materials using both types of specimens, as well as investigate repeatability with the high cycle specimen.

5.3 General fatigue life estimation

Materials and specimens used to determine general fatigue life are shown in Table 7. Some of the tests were done without fully reversible loading, due to the specifics of the testing technique, such as some ABI tests [61] or testing a wire specimen (Figure 13) as it would buckle [192]. Another interesting observation regarding fatigue life was that it can be predicted well when a single crystal of pure iron was tested as a representative sample of an extra-low carbon steel [123]. Small flat disc specimens (Figure 18 (c)) were determined to not be suitable as their results depended too much on stress concentrations making them unreliable [188]. Small round bar specimens (Figure 8 (b)), like their full-sized counterparts, experienced buckling with reversed loading. Small hourglass specimens (Figure 8 (c)) had a longer fatigue life than determined from a standard round bar specimen when a larger strain range was applied and shorter fatigue life when a smaller strain range was applied [156]. This makes it not suitable to consistently characterize the full fatigue life.

The effect of irradiation on fatigue life was investigated, the in-beam material had fatigue life extended by a factor of 2, while the post-irradiation material had fatigue life extended by a factor of 2.5 [128]. The effect of notches was investigated from two different angles. First one was the effect of surface roughness, where the roughness was considered to introduce notches. It was discovered that small polished specimens had a fatigue life closer to that of standard specimens than rougher specimens with roughness adjusted for [126]. The other angle was investigating the effect of nitriding on steel using small specimens. It was discovered that for smooth specimens nitriding increases fatigue life unless load amplitude was increased, but a notch significantly reduced fatigue life [151]. Also the fatigue life of the wire specimen was determined to be significantly longer than of a standard specimen, which meant that there was a significant size effect [192]. The high cycle specimen and the modified Krouse specimen both can be used to characterize the whole fatigue life curve, by applying a different stress range calculated according to beam deflection formula. As the stress values are calculated according to the deflection and applied load, it is very important for those to be measured accurately [186, 175]. Modified Krouse specimen was designed for testing additively manufactured material, the dual gauge providing a higher area and sensitivity to manufacturing defects [186].

Table 7: Materials and specimens from which general fatigue life estimation was acquired.

	Steels	Aluminium alloys	Nickel alloys	Titanium alloys
Sub-size standard specimens	[154, 176, 156, 126, 152, 61, 158]	[61]	[126]	[126]
Sub-size standard specimens (notched)	[123, 151, 128]			
Other specimens	[188, 192, 123, 61, 183, 186, 175, 106]	[61, 130]	[84, 107]	[83, 84]

Small punch fatigue testing looks like a promising technique for determining cyclic plasticity and fatigue life evaluation, however currently there are no correlations developed to actually calculate them [84, 83]. Cyclic ABI (constant load amplitude) testing is a promising technique for evaluating fatigue life, but, similarly to small punch fatigue testing, there currently is no way to convert the cyclic ABI life data to standard life data [106, 107]. Evaluating when exactly failure occurs is difficult in post-processing, therefore acoustic emission should be used instead [107].

Overall small specimens are capable of determining fatigue life. The main challenges with small specimen fatigue testing are the inconsistent size effects for certain geometries, difficult application of reversible loading and complicated methods required to interpret data. Some specimens cannot support reversible loading due to their geometry, as they buckle, requiring tensile-tensile loading, which causes ratcheting strain. This complicates their use for fatigue life characterization. The stress state in some specimens is multiaxial and the stress state in standard specimens is usually uniaxial, requiring complicated correlations between the two.

All small specimen fatigue testing techniques would benefit from investigations into repeatability, testing a wider variety of materials and limitations caused by microstructure. Testing techniques reliant on contact, such as such as small punch and ABI would benefit from an investigation into the effects of setup parameters.

Table 8: Materials and specimens from which fracture toughness was acquired.

	Steels	Aluminium alloys
Small punch specimens	[95, 67, 21, 55, 51, 75, 41, 74, 43, 56, 17, 99]	[26, 77]
Small punch specimens (notched)	[37, 91, 95, 94, 93, 89, 87, 99, 98, 96]	[97]
Small compact tension specimens	[161, 204, 207, 208, 160, 164, 166, 168, 167]	
3-point bending specimens	[137, 209, 139, 143, 163, 136, 146]	
Small Charpy specimens	[204, 147, 144, 164, 51, 148, 150]	
Indentation specimens	[100, 101, 117, 119]	
Bespoke specimens	[170]	

5.4 Other properties evaluated from fatigue testing

Other properties evaluated from small specimen fatigue testing include residual fatigue life, which has been evaluated for a nickel superalloy using sub-size standard specimens, however, due to low amounts of material available it was not directly verified by using standard specimens [124]. An ABI test was determined to be suitable to indicate fatigue damage for a set of various metallic materials, but not to quantify it [61]. Ratcheting was investigated using a wire specimen (Figure 13) made from stainless steel, and it was determined that ratcheting strain rate decreased when the number of cycles increased and the wire specimen had a strong memory of previous loading history [192].

6 Fracture testing

6.1 Fracture toughness

Materials and specimens for which fracture toughness have been determined are shown in Table 8. Bespoke specimens used were round specimens similar to a compact tension specimen with a side groove (Figure 25).

When the results from sub-size standard specimens were analysed, the effect of specimen size is inconsistent between different types of sub-size standard specimens. For CT specimens (Figure 19), some were reported to experience a size effect [161, 160, 164] and some were not [207, 208, 204], this appears to be dependent on the material being tested [168]. Also, using alternative methods to evaluate fracture toughness parameters improves the agreement between standard and sub-size CT specimen test results. A round robin experiment was performed for small CT specimens, it was discovered to be a robust technique, suitable to evaluate fracture toughness using the Master curve approach, with the distribution of the fracture toughness values being the same as for standard tests [167]. Considering the size effects for 3-point-bending specimens (Figure 20): in some cases the size effect was observed [163, 136] and in some cases it was not [209, 139, 143]. Similar observations were made for sub-size Charpy specimens. A model based on local approach to failure was extended to predict cleavage fracture and the effects of specimen geometry and constraint loss. The results are promising, however more research needs to be done to validate this model [150].

Regarding small punch specimens, fracture toughness was determined from correlations between fracture toughness of the bulk material and defect opening displacement [95, 37, 94, 91], equivalent fracture strain [67, 21, 41, 26] or fracture strain [51, 74]. As for indirect methods, FEA was used in order to calculate the J-integral which was then used to evaluate fracture toughness [94, 93]. J-integral is a path independent line integral around the crack tip, used to calculate the strain energy release rate per unit surface fracture area. Energy methods were also used, by evaluating the area under the force-displacement curve from small punch test results, which was then used to evaluate the J-integral [94, 43]. This approach yielded more robust results than using FEA or defect opening displacement approach. A failure assessment diagram could be used in order to evaluate material stress intensity factor which was then used to calculate fracture toughness, which depended on the level of the diagram and initial crack size and specimen thickness ratio[87]. Without checking against standard test results, bending theory was used to evaluate the fracture toughness of a thin plate with a through thickness crack [99]. A very indirect method was the usage of neural networks to get parameters for a damage model from small punch testing results, then using those parameters to simulate a CT test and using that to get fracture toughness, with a reasonably good agreement to standard test data [56, 17].

Other observations related to small punch fracture toughness testing were that the pre-cracking method did not have a significant effect on the evaluated fracture toughness [89]. Due to plane strain state in the specimen a circular notch should allow to evaluate fracture toughness of brittle materials [98], which was identified as impossible using a notch through thickness due to not uniform stress state [37]. An investigation was done into what effect the dimensions of the small punch testing setup have on the testing results [75]. It was discovered using FEA that when the punch ball was too large or the lower die was too small the fracture toughness identified by the test was inaccurate, however, some of this could have been caused by model and calculation assumptions. In order to get good agreement between bulk material fracture toughness test results and small punch test results the centre hole of the lower die should be 1.5-2 times larger than the ball [75]. In one study a small dog-bone specimen was used instead of the usual small punch specimen, with

varying section widths. It was discovered that the section width of 4 mm and using 70% load based fracture energy for J-integral results in the best agreement with standard CT specimen results [77].

As for other specimens, the round specimen with side-grooves [170] behaves just like a Charpy specimen in every way, however the fracture toughness at a critical depth is higher than in a Charpy specimen. As for ABI tests, fracture toughness is determined using continuum damage mechanics and is in good agreement with results from standard tests [100, 101]. The effects of machining parameters on fracture toughness can be investigated using ABI [117] and the technique can be used to successfully test the fracture toughness of in service components by using a portable testing machine [119].

A future direction of testing for fracture toughness using small specimens should involve investigating whether the testing techniques developed are suitable for a wider variety of materials.

6.2 Ductile to brittle transition temperature

Ductile to brittle transition temperature (DBTT) was investigated for materials and specimens listed in Table 9. Generally DBTT determined from small punch specimens was lower than determined from standard specimens [95, 43, 98], which was speculated to had been caused by a combination of size effects and strain rates. Depending on microstructure, notches can raise DBTT [92], however notched small punch specimens were not used to determine DBTT due to the effect being microstructure dependent and DBTT being lower than Charpy DBTT even with the notch. Due to a linear correlation between small punch DBTT and Charpy DBTT small punch test data can be used to evaluate bulk DBTT provided the material is isotropic [19, 210]. The effect of small punch test machine dimensions was investigated, it was discovered that punch diameter had a significant effect, mainly if it is too small it can cause brittle failure [25]. A possible advantage of small punch testing, found in one study, could be that the scatter of DBTT values was approximately half of the scatter from Charpy testing [27]. DBTT shift due to helium ions causing irradiation damage was investigated using small punch specimens and it was discovered that there was essentially no effect [73].

Sub-size standard specimens were mostly used to study embrittlement due to processing environment, such as liquid metal embrittlement, helium embrittlement [140], effect of sulphur on DBTT of polycrystalline nickel [145] or effect of phosphorus on DBTT in reduced activation ferritic steel and the possibility to use that to simulate non-hardening embrittlement [204]. The dependence of DBTT on v-notch dimensions when sub-size Charpy specimens were tested was investigated [142]. It was discovered that DBTT could be almost uniquely determined by a ratio between notch depth and notch root radius or elastic stress concentration factor, therefore appropriately sized notches need to be used for small specimen DBTT to be representative of bulk DBTT. As the CT specimen size increases the DBTT increases as well, however that can be accounted for using a model [165].

Table 9: Materials and specimens from which ductile to brittle transition temperature was determined.

	Steels	Nickel alloys
Small punch specimens	[19, 25, 210, 43, 27, 73, 95, 149]	
Small punch specimens (notched)	[95, 98]	
Small compact tension specimens	[204, 73, 165]	
3 point bending specimens		[145]
Small Charpy specimens	[73, 19, 140, 204, 142]	

Overall, neither small punch specimens nor sub-size standard specimens are particularly suitable to evaluate DBTT, as one of them underestimates it and the other overestimates it, however, both can be used as ranking tools and DBTT can be evaluated using correlations. In order to further the research into DBTT it would be beneficial to investigate repeatability and the suitability of the correlations for different materials.

6.3 Fracture appearance transition temperature

Fracture appearance transition temperature (FATT) was investigated for steels exclusively [23, 92, 95, 28, 36] using small punch specimens. One of the specimens had a semi-circular notch (Figure 23 (c)) [92] and another had a notch through thickness (Figure 22 (a)) [95].

Overall, it seems that small punch specimens could be used to determine FATT, but it was always lower than FATT from Charpy tests. Notches generally lowered FATT in SPT, but not enough to reach Charpy FATT [92]. Since FATT from small punch specimens and Charpy specimens was linearly correlated, small punch test results could be used to estimate bulk FATT [36]. It was observed that irradiation shifted FATT estimated from SPT results to higher temperatures for ferritic materials [23] which generally agreed with standard specimen testing results.

6.4 Damage model parameters

Damage model parameters were exclusively evaluated for steels [86, 88, 57, 17, 16, 31] using small punch testing,

one of the small punch specimens used had a notch through length (Figure 23) [86].

Two models were considered: Gurson-Tvergaard [88] and Gurson-Tvergaard-Needleman [86, 57, 16, 17]. Two methods were used to obtain the material model parameters: neural networks trained on a database of systematically varied material parameters [16, 17] and FEA simulation fitting the model parameters [88, 86, 57].

Two approaches to the neural network method were attempted: neural network approximated the inverse problem to the FEA solution and gave the material parameters as an answer or neural network approximated the FEA solution directly and damage model parameters were identified by conjugate directions finding algorithm. The results from the second method agreed with the results from standard specimens better, making it more suitable for this problem [16]. This method was further validated with additional testing [17].

FEA simulation method was validated by simulating small punch tests and comparing the resulting force-displacement curves to experimentally obtained force-displacement curves. Two methods of fitting some of the damage model parameters were investigated: desirability method and Pareto front method. Desirability method solved a one-dimensional problem in order to determine the parameters while Pareto front method solved a two-dimensional problem. Pareto front was identified to be better as the global error from it was smaller [88]. Good agreement was found between simulated force-displacement curves and experimentally acquired force- displacement curves.

Overall, at least for steels and the damage models investigated, the parameters can be determined using small punch testing and there are various methods to determine them. Good agreement with standard methods was found in all cases.

6.5 Other properties evaluated from fracture testing

Other fracture related property that was investigated was the effect of liquid metal embrittlement on ductile to brittle transition in steel [76]. It was discovered that the strain rate was the most important parameter as exposure time directly depended on it. Similarly to fracture toughness, tear toughness testing using small specimens (Figure 21) was investigated, though so far it only appears to be suitable for ranking [190]. The strength of a HIP joint was investigated using a torsion test specimen (Figure 24)[179, 180]. The technique was identified as a promising potential replacement of Charpy impact tests. Castelluccio attempted to characterize fracture toughness using crack tip opening displacement in-situ testing, it was only successful for ranking the initial part of the resistance curves [138]. Work hardening was found to have a significant effect on the tearing resistance of small CT specimen test results [168].

Table 10: Materials and specimens from which crack initiation properties were determined.

	Steels	Nickel alloys	Titanium alloys
Sub-size standard specimens	[123, 128, 133]	[125]	[134]
Small punch specimens	[89]		
Other specimens	[178, 183]		

7 Crack growth

7.1 Crack initiation

Materials and specimens used for small specimen crack initiation testing are listed in Table 10.

Crack initiation has mostly been observed by performing a tensile test and observing when and where the cracks would initiate [125, 123, 128, 178]. In the nickel superalloy, they initiated at specimen surface, grain boundaries weakened by oxidation and interdendritic regions with micropores, which was the same as in full size specimens [125]. In a ferritic ductile cast iron the cracks tend to nucleate along the nodule-matrix interface and the first to freeze zones [133]. It was discovered that for 316 stainless steel irradiation retarded crack initiation [128]. Sharp crack tip was identified to be better than rounded notch for pre-cracking a small punch specimen, as it more closely resembled the crack in a CT specimen [89]. Hayakawa investigated the effect of crack initiation on crystal misorientation using small fatigue specimens (Figure 27 (a)) and discovered that both grain reference orientation deviation and crystal misorientation increased at initiation, then remained constant [178]. When investigating the behaviour of a single crystal crack initiation it was discovered that a slip system activated, initiated the crack, which caused a multiaxial stress state, which then activated a different slip system [123]. For sub-size standard specimens with the same microstructure the cracks initiated in exactly the same way as in standard-sized specimens [134]. For the hydraulic bulge fatigue test, the cracks always initiate on the flat side of the specimen [183].

Scanning electron microscope (SEM) was primarily used for investigating crack initiation [123, 125, 89, 183, 133, 134], in particular the location where the crack initiated. The number of cycles to crack initiation was defined either as a number of cycles when a crack or a slip greater than the grain size was observed using a microscope after an interrupted test and polishing the surface [178] or by combining initiation and growth up to 100 microns due to SEM resolu-

tion, then subtracting the number of visible striations in the specimen from the number of cycles to failure [128].

Overall, in some cases crack initiation found using small specimens is representative of bulk material, in other cases small specimens were used for better visibility of crack initiation due to their size.

7.2 Crack propagation

Materials and specimens used for small specimen crack propagation testing are listed in Table 11. Cracks in the nickel superalloy propagated in the interdendritic region, the propagation mode on the surface was transgranular and the overall behaviour was similar to virgin material under same fatigue loading conditions [125]. For the ferritic ductile cast iron, cracks prefer to propagate along the same areas as they tend to initiate [133]. Irradiation was discovered to retard crack propagation similarly to how it retarded crack initiation [128]. Kovarik developed a method for measuring the crack propagation rate using mini cantilever specimens and a resonance fatigue test method with micrometric resolution, measuring the crack propagation using a compliance technique [141]. Crack growth rates comparable to rates in standard tests can be achieved. A CIET specimen (Figure 27 (c)) was identified to be very suitable for crack propagation testing as the results matched the results from a standard test well after correcting for crack closure effects [181]. The same observation was also made regarding two sub-size standard specimens [191, 162]. Cracks were discovered to propagate faster though closely spaced stringers and small voids, due to closely spaced stringers having higher stress concentration between them [211]. When sub-size standard specimens were tested with the same microstructure as standard specimens, the cracks propagated in the same way [134].

An interesting testing method was developed in order to study short stage 1 cracks in situ, based on diffraction contrast tomography and synchrotron tomography [153]. Kim used a load separation method to measure the crack propagation and d-c potential drop method to verify it [169]. De investigated the effect of friction stir processing on the crack propagation using SEM and discovered that crack propagation rate in microstructurally small crack regime was reduced due to grain boundaries acting as barriers, while in physically small crack regime they deflected cracks and increased the difficulty of slip [174]. When hydraulic bulge fatigue testing is performed, the crack propagates from the flat side of the specimen to the concave side, then a chip forms and the specimen fails [183]. Small punch specimens tested under cyclic loading conditions fail with a star shaped pattern radiating from the middle of the contact area. Striations cannot be seen when the loading is reversed as crack closure erases them [83, 84].

Other methods used to investigate crack propagation were calculating the crack width from the crack opening displacement gauge measurements [191], using a travelling microscope with a digital image capturing device [162], using a compliance technique using crack mouth opening displacement and load [181] and using a standard procedure from the slope of the unloading line [211]. Crack propagation velocity can be calculated from the duration of impact and the length of fracture zones [149].

Overall, small specimens offer the possibility to study stage 1 cracks and can be used to get bulk crack propagation data after adjusting for crack closure effects. The gaps in the current research are the investigation of repeatability of crack propagation studies and measuring crack propagation for a wider variety of materials.

8 Conclusions

From the literature reviewed in this paper, the following conclusions can be made:

- It is clear there is significant, worldwide interest in small punch testing for a wide variety of material properties and from a wide variety of industries with vastly different applications. Several of the existing test techniques are used heavily in order to provide vital material properties and to perform ranking/health check exercises where standard test techniques are not viable due to material quantities available.
- Of the material properties discussed in this paper, fracture toughness has received the most interest, followed by yield strength and ultimate tensile strength, where specimens tailored for a specific application are common.
- Small specimens offer advantages for certain types of testing, such as when temperature control is of interest, as well as challenges for others, such as fracture toughness due to size effects.
- In some cases, without further development, and depending on the information required, some specimen types may not be suitable, and so care needs to be taken before deciding if a small specimen technique is applicable. For example, certain materials do not exhibit a limit load making small punch not suitable for testing them for yield strength.
- However, several small specimen techniques can be used in certain applications with extremely positive results, in particular, when sub-size specimens are tested for tensile and fatigue properties.
- An appropriate manufacturing method needs to be chosen to manufacture small specimens as a hardened surface layer can affect results significantly.

Table 11: Materials and specimens from which crack propagation properties were determined.

	Steels	Aluminium alloys	Nickel alloys	Magnesium alloys	Zirconium alloys	Zinc alloys	Titanium alloys
Sub-size standard specimens	[128, 141, 191, 162, 133, 149]	[141, 162]	[125]	[153]		[134]	
Altered sub-size standard specimens					[211]	[169]	
Bespoke specimens	[181, 183]	[174, 181]	[84]				[84, 83]

- A standard publication is in progress for the Small Punch specimen type, while other small specimen techniques are not currently close to standardisation.
- Sub-size standard specimen test results tend to produce results the most similar to standard specimen test results, likely due to well established data interpretation techniques.
- The need for further development of specimen types and test types that these specimen types are applicable to is abundant. As a result, the authors suggest the following direction of travel for further progress in the field of small specimen testing.
  - A wider variety of materials should be tested, especially for methods that rely on correlations in order to develop material independent correlations
  - A more consistent investigation of surface roughness effects should be done
  - A more thorough investigation into grain size effects, as they appear to be underinvestigated for several types of specimens and testing
  - A thorough investigation into repeatability of small specimen testing techniques should be done

Acknowledgements The authors would like to thank the Engineering and Physical Sciences Research Council (EPSRC) for the funding this work through the Centre for Doctoral Training in Innovative Metal Processing (IMPaCT). EPSRC reference number: EP/L016206/1.

Conflict of interest

The authors declare that they have no conflict of interest.

Declarations

Funding

Engineering and Physical Sciences Research Council (EPSRC) funded this work through the Centre for Doctoral Training in Innovative Metal Processing (IMPaCT). EPSRC reference number: EP/L016206/1.

Conflicts of interest

The authors declare that they have no conflict of interest.

Availability of data

Not applicable

Code availability

Not applicable

Authors contributions

All authors contributed to the review conception and structuring. Literature search, data analysis and the first draft were performed by Julija Kazakeviciute. All authors commented on previous versions of the manuscript. All authors read and approved the final manuscript.

References

1. C.C. Dyson, W. Sun, C.J. Hyde, S.J. Brett, and T.H. Hyde. Use of small specimen creep data in component life management: a review. *Mater Sci Tech-Lond*, 32 (15):1567–1581, 2016.
2. T.H. Hyde, W. Sun, and J.A. Williams. Requirements for and use of miniature test specimens to provide mechanical and creep properties of materials: A review. *Int Mater Rev*, 52(4):213–255, 2007.
3. J.P. Rouse, F. Cortellino, W. Sun, T.H. Hyde, and J. Shingledecker. Small punch creep testing: Review on modelling and data interpretation. *Mater Sci Tech-Lond*, 29(11):1328–1345, 2013.
4. P. Hosemann, C. Shin, and D. Kiener. Small scale mechanical testing of irradiated materials. *J Mater Res*, 30(9):1231–1245, 2015.
5. T. Connolley, P.E. Mchugh, and M. Bruzzi. A review of deformation and fatigue of metals at small size scales. *Fatigue Fract Eng Mater*, 28(12):1119–1152, 2005.
6. P. Zheng, R. Chen, H. Liu, J. Chen, Z. Zhang, X. Liu, and Y. Shen. On the standards and practices for miniaturized tensile test – a review. *Fusion Eng Des*, 161, 2020.

7. A. Kolhatkar, V. Karthik, G.M.S.K. Chaitanya, A. Kumar, and D. Ramchandran. Development and validation of a miniature tensile specimen for determination of mechanical properties. *J Test Eval*, 47(5), 2019.
8. J.D. Lord, B. Roebuck, R. Morrell, and T. Lube. 25 year perspective: Aspects of strain and strength measurement in miniaturised testing for engineering metals and ceramics. *Mater Sci Technol*, 26(2):127–148, 2010.
9. S. Arunkumar. Overview of small punch test. *Metal Mater Int*, 2019.
10. Baldev Raj V. Karthik, K.V. Kasiviswanathan. *Miniaturized Testing of Engineering Materials*. CRC Press, 1st edition, 2016.
11. E. Lucon. Testing of small-sized specimens. *Comprehensive Materials Processing*, 1:135–163, 05 2014.
12. H. Liu, R. Chen, M. Wen, L. Zhang, and Y. Shen. Optimizing parallel section length for small tensile specimen with fabrication non-uniformity in thickness. *Fusion Eng Des*, 147, 2019.
13. G. E. Lucas, G. R. Odette, and J. W. Sheckherd. *The Use of Small-Scale Specimens for Testing Irradiated Material, ASTM STP S88*. American Society for Testing and Materials, Philadelphia, 1986. pp. 112-140.
14. J.M. Alegre and I.I. Cuesta. Determination of the fracture toughness of the 15.5-PH steel using pre-cracked small punch tests. In *18th European Conference on Fracture: Fracture of Materials and Structures from Micro to Macro Scale*, 2010.
15. H. R. Abedi, A. Zarei-Hanzaki, E. Karimi, and N. Haghdadi. The shear punch jump test - a novel application of a small specimen testing technique for rapid evaluation of deformation mechanisms. *Exp Mech*, 55(8):1569–1573, 2015.
16. M. Abendroth and M. Kuna. Determination of ductile material properties by means of the small punch test and neural networks. *Adv Eng Mater*, 6(7):536–540, 2004.
17. M. Abendroth and M. Kuna. Identification of ductile damage and fracture parameters from the small punch test using neural networks. *Eng Frac Mech*, 73(6): 710–725, 2006.
18. Martin Abendroth and Stefan Soltysiak. Assessment of material properties by means of the small punch test. In *Recent Trends in Fracture and Damage Mechanics*, pages 127–157, 2016. ISBN 978-3-319-21467-2.
19. E. Altstadt, M. Serrano, M. Houska, and A. García-Junceda. Effect of anisotropic microstructure of a 12Cr-ODS steel on the fracture behaviour in the small punch test. *Mat Sci Eng A-Struct*, 654:309–316, 2016.
20. S. Arunkumar and Raghu V. Prakash. Estimation of tensile properties of pressure vessel steel through automated ball indentation and small punch test. *T Indian I Metals*, 69(6):1245–1256, 2016.
21. M.M. Assas, A. Husain, and D.K. Sehgal. Identification of mechanical characteristics of materials using diminutive specimen - an empirical study. In *Procedia Engineer*, volume 10, pages 3109–3116, 2011.
22. P.M. Bravo Díez, M. Preciado Calzada, D. Cárdenas Gonzalo, and J. Calaf Chica. Change of mechanical properties of AM60B alloy with heat treatments and its correlation with small punch tests. *Theor Appl Fract Mec*, 86(A):101–108, 2016.
23. M. Březina, J. Petzová, L. Kupča, and M. Kapusňák. Utilization of SPT techniques for evaluation of changes in the properties of the VVER-440 reactor pressure vessel steels after their irradiation in the research and power reactors. In *Pres Ves P*, volume 1A, 2015. ISBN 9780791856925.
24. M. Bruchhausen, J-. M. Lapetite, S. Ripplinger, and T. Austin. Small punch tensile/fracture test data and 3D specimen surface data on Grade 91 ferritic/martensitic steel from cryogenic to room temperature. *Data in Brief*, 9(Supplement C):245 – 251, 2016.
25. M. Bruchhausen, S. Holmström, I. Simonovski, T. Austin, J.-M. Lapetite, S. Ripplinger, and F. de Haan. Recent developments in small punch testing: Tensile properties and DBTT. *Theor Appl Fract Mec*, 86:2–10, 2016.
26. E. Budzakoska, D.G. Carr, P.A. Stathers, H. Li, R.P. Harrison, A.K. Hellier, and W.Y. Yeung. Predicting the J integral fracture toughness of Al 6061 using the small punch test. *Fatigue Fract Eng Mater*, 30(9):796–807, 2007.
27. J.H. Bulloch. The small punch toughness test: some detailed fractographic information. *Int J Pres Ves Pip*, 63(2):177–194, 1995.
28. J.H. Bulloch. A review of the ESB small punch test data on various plant components with special emphasis on fractographic details. *Eng Fail Anal*, 9(5):511–534, 2002.
29. J.H. Bulloch. A study concerning material fracture toughness and some small punch test data for low alloy steels. *Eng Fail Anal*, 11(4):635–653, 2004.
30. J.S. Cheon and I.S. Kim. Evaluation of thermal aging embrittlement in CF8 duplex stainless steel by small punch test. *J Nucl Mater*, 278(1):96–103, 2000.
31. I.I. Cuesta, J.M. Alegre, and H. Barbáchano. Use of the Gurson-Tvergaard-Needleman (GTN) damage model to simulate small punch test on pre-cracked specimens [Aplicación del modelo de daño de Gurson-Tvergaard-Needleman (GTN) para la simulación del ensayo miniatura de punzonado sobre probetas prefisuradas]. *Rev Metal Madrid*, 46(Extra):53–63, 2010.

32. I.I. Cuesta and J.M. Alegre. Hardening evaluation of stamped aluminium alloy components using the small punch test. *Eng Fail Anal*, 26:240–246, 2012.
33. S. Davies, S. Jeffs, R. Lancaster, and G. Baxter. High temperature deformation mechanisms in a DLD nickel superalloy. *Materials*, 10(5):457, 2017.
34. M. Fernández, C. Rodríguez, F.J. Belzunce, and T.E. García. Mechanical behaviour estimation of synchronizer hubs using miniaturized specimens. In *Proceedings Euro PM 2015: International Power Metallurgy Congress and Exhibition*, 2015. ISBN 9781899072477.
35. E. Fleury and J.S. Ha. Small punch tests to estimate the mechanical properties of steels for steam power plant: I. Mechanical strength. *Int J Pres Ves Pip*, 75(9):699–706, 1998.
36. J. Foulds and R. Viswanathan. Determination of the toughness of in-service steam turbine disks using small punch testing. *J Mater Eng Perform*, 10(5):614–619, 2001.
37. T.E. García, C. Rodríguez, F.J. Belzunce, and C. Suárez. Estimation of the mechanical properties of metallic materials by means of the small punch test. *J Alloy Compd*, 582:708–717, 2014.
38. T.E. García, C. Rodríguez, F.J. Belzunce, I. Peñuelas, and B. Arroyo. Development of a methodology to study the hydrogen embrittlement of steels by means of the small punch test. *Mat Sci Eng A-Struct*, 626: 342–351, 2015.
39. T.E. García, B. Arroyo, C. Rodríguez, F.J. Belzunce, and J.A. Álvarez. Small punch test methodologies for the analysis of the hydrogen embrittlement of structural steels. *Theor Appl Fract Mec*, 86:89–100, 2016.
40. H. Ge, Q. Huang, J. Xin, and K. Sun. Small specimen test techniques applied to evaluate the mechanical properties of CLAM steel. *J Fusion Energ*, 34(5): 1124–1128, 2015.
41. K. Guan, L. Hua, Q. Wang, X. Zou, and M. Song. Assessment of toughness in long term service CrMo low alloy steel by fracture toughness and small punch test. *Nucl Eng Des*, 241(5):1407–1413, 2011.
42. K. Guan, J. A. Szpunar, K. Matocha, and D. Wang. Study on temper embrittlement and hydrogen embrittlement of a hydrogenation reactor by small punch test. *Materials*, 10(6):671, 2017.
43. J.S. Ha and E. Fleury. Small punch tests to estimate the mechanical properties of steels for steam power plant: II. Fracture toughness. *Int J Pres Ves Pip*, 75(9):707–713, 1998.
44. R. Hu and X. Ling. Three-dimensional numerical simulation on plastic damage in small punch specimen of Zirconium. *Int J Pres Ves Pip*, 86(12):813–817, 2009.
45. R. C. Hurst and K. Matocha. A Renaissance in the use of the small punch testing technique. In *ASME Pressure and Piping Conference - 2015, Vol 1B*, 2015. ISBN 978-0-7918-5693-2.
46. A. Husain, D.K. Sehgal, and R.K. Pandey. An inverse finite element procedure for the determination of constitutive tensile behavior of materials using miniature specimen. *Comp Mater Sci*, 31(1-2):84–92, 2004.
47. J. Isselin and T. Shoji. Yield strength evaluation by small-punch test. *J Test Eval*, 37(6):531–537, 2009.
48. C. Kannan, S. Bhattacharya, D.K. Sehgal, and R.K. Pandey. Effect of specimen thickness and punch diameter in evaluation of small punch test parameters toward characterization of mechanical properties of Cr-Mo steels. *J Test Eval*, 42(6), 2014.
49. V. Karthik, K. Laha, P. Parameswaran, K. V. Kasiviswanathan, and Baldev Raj. Small specimen test techniques for estimating the tensile property degradation of mod 9Cr-1Mo steel on thermal aging. *J Test Eval*, 35(4):438–448, 2007.
50. I. Klevtsov, A. Dedov, and A. Molodtsov. Measurement of the tensile and yield strength of boiler steels by small punch and tensile test methods [aurukatlateraste tõmbetugevuse ja voolepiiri mõõtmine kuuliga surumise ning tõmbekatse meetodil]. *Estonian Journal of Engineering*, 15(2):99–107, 2009.
51. P. Konopik, J. Dzugan, and M. Rund. Determination of fracture toughness in the upper shelf region using small sample test techniques. In *Metal 2015: 24th International Conference on Metallurgy and Materials*, pages 710–715, 2015. ISBN 978-80-87294-62-8.
52. K. Kumar, A. Pooleery, K. Madhusoodanan, R.N. Singh, J.K. Chakravartty, R.S. Shriwastaw, B.K. Dutta, and R.K. Sinha. Evaluation of ultimate tensile strength using miniature disk bend test. *J Nucl Mater*, 461:100–111, 2015.
53. R. Lacalle, J.A. Álvarez, and F. Gutiérrez-Solana. Analysis of key factors for the interpretation of small punch test results. *Fatigue Fract Eng Mater*, 31(10): 841–849, 2008.
54. T. Linse and M. Kuna. Characterization of reactor vessel steels in the brittle-ductile transition region. In *17th European Conference on Fracture 2008: Multilevel Approach to Fracture of Materials, Components and Structures*, volume 1, pages 765–772, 2008. ISBN 9781617823190.
55. T. Linse, M. Kuna, J. Schuhknecht, and H.-W. Viehrig. Application of the small-punch test to irradiated reactor vessel steels in the brittle-ductile transition region. *J ASTM Int*, 5(4), 2008.
56. T. Linse, M. Kuna, and H.-W. Viehrig. Quantification of brittle-ductile failure behavior of ferritic reactor pressure vessel steels using the small-punch-test

and micromechanical damage models. *Mat Sci Eng A-Struct*, 614:136–147, 2014.

57. M. Madia, S. Foletti, A. Cammi, and G. Torsello. Characterization of the fracture behaviour of a turbine rotor steel by means of the small punch test. In *18th European Conference on Fracture: Fracture of Materials and Structures from Micro to Macro Scale*, 2010.
58. J. Mak, T. Wei, R. Wuhrer, W. Yeung, G. Heness, and Z. Di. A solution for estimating the tensile yield strength from small specimens. *J Test Eval*, 41(4): 647–650, 2013.
59. K. Milička and F. Dobeš. Small punch testing of P91 steel. *Int J Pres Ves Pip*, 83(9):625–634, 2006.
60. S.D. Norris and J.D. Parker. Deformation processes during disc bend loading. *Mater Sci Tech Ser*, 12(2): 163–170, 1996.
61. R.V. Prakash and A. Subbiah. Evaluation of fatigue data through miniature specimen test techniques. In *Pres Ves P*, volume 1A, 2015. ISBN 9780791856925.
62. R. V. Prakash and S. Arunkumar. Influence of friction on the response of small punch test. *T Indian I Metals*, 69(2):617–622, 2016.
63. R. V. Prakash, T. Ramesh, N. Raju, and S. Suresh. Correlation of tensile properties of pressure vessel steels by shear punch and small punch test methods. In *International Mechanical Engineering Congress and Exposition - 2012, Vol 3, Pts A-C: Design, Materials and Manufacturing*, pages 635–640, 2013. ISBN 978-0-7918-4519-6.
64. T. Ramesh, R.V. Prakash, S. Suresh, and N. Raju. Evaluation of tensile properties of pressure vessel materials by shear punch test method. *Appl Mech Mater*, 187:53–57, 2012.
65. C. Rodríguez, J. García Cabezas, E. Cárdenas, F.J. Belzunce, and C. Betegón. Mechanical properties characterization of heat-affected zone using the small punch test. *Weld J*, 88(9):188–192, 2009.
66. M. Sanders, F. Di Bella, and H. Liang. Small-scale mechanical characterization of aluminum and titanium alloys. *J Test Eval*, 39(1):9–15, 2011.
67. M.L. Saucedo-Muñoz, T. Hashida, and V.M. Lopez-Hirata. Correlationship between J ICand equivalent fracture strain determined by small-punch test in JN1, JJ1 an JK2 austenitic stainless steels. In *TMS Annual Meeting*, pages 487–494, 2012. ISBN 9781118291221.
68. J. Siegl, P. Haušild, A. Janča, R. Kopřiva, and M. Kytka. Characterisation of mechanical properties by small punch test. *Key Eng Mat*, 606:15–18, 2014.
69. I. Simonovski, S. Holmström, and M. Bruchhausen. Small punch tensile testing of curved specimens: Finite element analysis and experiment. *Int J Mech Sci*, 120(Supplement C):204 – 213, 2017.
70. M. Song, K. Guan, W. Qin, J.A. Szpunar, and J. Chen. Size effect criteria on the small punch test for AISI 316L austenitic stainless steel. *Mat Sci Eng A-Struct*, 606:346–353, 2014.
71. D. Sunjaya, T. Wei, R. Harrison, and W.Y. Yeung. Finite element modelling of small punch test on 304H stainless steel. *Key Eng Mat*, 345-346:1165–1168, 2007.
72. S. Szávai, P. Rózsahegyi, J. Dudra, R. Beleznai, Z. Bézi, and S. Jónás. Determination of mechanical properties of operating components using instrumented hardness testing, small punch and small size tensile testing techniques. *Lecture Notes in Mechanical Engineering*, pages 135–150, 2017.
73. E. Wakai, H. Ohtsuka, S. Matsukawa, K. Furuya, H. Tanigawa, K. Oka, S. Ohnuki, T. Yamamoto, F. Takada, and S. Jitsukawa. Mechanical properties of small size specimens of F82H steel. *Fusion Eng Des*, 81(8-14 Part B):1077–1084, 2006.
74. Z.-X. Wang, H.-J. Shi, J. Lu, P. Shi, and X.-F. Ma. Small punch testing for assessing the fracture properties of the reactor vessel steel with different thicknesses. *Nucl Eng Des*, 238(12):3186–3193, 2008.
75. S. Yang, Z. Yang, and X. Ling. Fracture toughness estimation of ductile materials using a modified energy method of the small punch test. *J Mater Res*, 29(15): 1675–1680, 2014.
76. C. Ye, J.-B. Vogt, and I. Proriol Serre. Liquid metal embrittlement of the T91 steel in lead bismuth eutectic: The role of loading rate and of the oxygen content in the liquid metal. *Mat Sci Eng A-Struct*, 608:242–248, 2014.
77. I.I. Cuesta, A. Willig, A. Díaz, E. Martínez-Pañeda, and J.M. Alegre. Pre-notched dog bone small punch specimens for the estimation of fracture properties. *Eng Fail Anal*, 96:236–240, 2019.
78. P. Maksimkin, S.V. Ruban, Y.Y. Nurgaly, and M.P. Short. Studying the changes in the mechanical properties of neutron-irradiated chromium-nickel steels using the “shear punch” method. *Prob At Sci Tech*, 120 (2):82–90, 2019.
79. E. Priel, B. Mittelman, S. Haroush, A. Turgeman, R. Shneck, and Y. Gelbstein. Estimation of yield and ultimate stress using the small punch test method applied to non-standard specimens: A computational study validated by experiments. *Int J Mech Sci*, 135: 484–498, 2018.
80. P. Konopik, R. Prochazka, M. Rund, and J. Dzugan. Novel methods for high-cycle fatigue life determination. *Key Eng Mat*, 810:40–45, 2019.
81. H.T. Pham and T. Iwamoto. An evaluation of fracture properties of type-304 austenitic stainless steel at high deformation rate using the small punch test. *Int J Mech*

Sci, 144:249–261, 2018.

82. M.D. Richardson, S. Connolly, M. Gorley, B.P. Wynne, and E. Surrey. Influence of surface finish on small punch testing of 9Cr Eurofer-97 steel. *J Test Eval*, 48(2), 2020.
83. R.J. Lancaster, S.P. Jeffs, H.W. Illsley, C. Argyrakis, R.C. Hurst, and G.J. Baxter. Development of a novel methodology to study fatigue properties using the small punch test. *Mat Sci Eng A-Struct*, 748:21–29, 2019.
84. D.T.S. Lewis, R.J. Lancaster, S.P. Jeffs, H.W. Illsley, S.J. Davies, and G.J. Baxter. Characterising the fatigue performance of additive materials using the small punch test. *Mat Sci Eng A-Struct*, 754:719–727, 2019.
85. R. Kopriva, M. Brumovský, M. Kytka, M. Lasan, J. Siegl, and K. Matocha. *Application of Miniature Small Punch Test Specimen in Determination of Tensile Properties*, pages 1–8. 04 2015. ISBN 978-0-8031-7597-6.
86. J.M. Alegre, I.I. Cuesta, and P.M. Bravo. Implementation of the GTN damage model to simulate the small punch test on pre-cracked specimens. In *Procedia Engineer*, volume 10, pages 1007–1016, 2011.
87. I.I. Cuesta and J.M. Alegre. Determination of the fracture toughness by applying a structural integrity approach to pre-cracked small punch test specimens. *Eng Frac Mech*, 78(2):289–300, 2011.
88. I.I. Cuesta, J.M. Alegre, and R. Lacalle. Determination of the Gurson-Tvergaard damage model parameters for simulating small punch tests. *Fatigue Fract Eng Mater*, 33(11):703–713, 2010.
89. I.I. Cuesta, C. Rodriquez, F.J. Belzunce, and J.M. Alegre. Analysis of different techniques for obtaining precracked/notched small punch test specimens. *Eng Fail Anal*, 18(8):2282–2287, 2011.
90. T.E. García, C. Rodríguez, F.J. Belzunce, I. Pe nuelas, and I.I. Cuesta. Estimation of the fracture toughness of structural steels by means of the CTOD evaluation on notched small punch specimens. *Proc Mat Sci*, 3 (Supplement C):861 – 866, 2014.
91. T.E. García, C. Rodríguez, F.J. Belzunce, and I.I. Cuesta. Development of a new methodology for estimating the CTOD of structural steels using the small punch test. *Eng Fail Anal*, 50:88–99, 2015.
92. K. Matocha, O. Dorazil, and R. Hurst. The present SP tests for determining the transition temperature TSP on "U" notch disc specimens. *Materials*, 10(5):87–93, 2017.
93. Y. Xu and K. Guan. Evaluation of fracture toughness by notched small punch tests with Weibull stress method. *Mater Design*, 51:605–611, 2013.
94. J.M. Alegre, I.I. Cuesta, and H.L. Barbachano. Determination of the fracture properties of metallic materials using pre-cracked small punch tests. *Fatigue Fract Eng Mater*, 38(1):104–112, 2015.
95. R. Lacalle, D. Andrés, J.A. Álvarez, and F. Gutiérrez-Solana. Transition region of nuclear vessel steels: Master curve approach using small punch notched specimens. *Key Eng Mat*, 734:77–86, 2017.
96. B. Arroyo, J.A. Álvarez, R. Lacalle, P. González, and F. Gutiérrez-Solana. Using small punch tests in environment under static load for fracture toughness estimation in hydrogen embrittlement. In *IOP Conference Series: Materials Science and Engineering*, volume 272, 2017.
97. S.J. Eck and A.J. Ardell. Fracture toughness of Ti-46·5Al-2·1Cr-3·0Nb-0·2W from finite element analysis of miniaturized disk-bend test results. *Intermetallics*, 6(6):471–477, 1998.
98. K. Turba, B. Gülçimen, Y.Z. Li, D. Blagoeva, P. Hähner, and R.C. Hurst. Introduction of a new notched specimen geometry to determine fracture properties by small punch testing. *Eng Frac Mech*, 78(16):2826–2833, 2011.
99. J.-B. Ju and D. Kwon. Assessment of fracture characteristics from revised small punch test using precracked specimen. *Metal Mater Int*, 4(4):742–746, 1998.
100. S. Ghosh, S. Yadav, and G. Das. Ball indentation technique: A currently developed tool to study the effect of various heat treatments on the mechanical properties of EN24 steel. *Mater Lett*, 62(24):3966–3968, 2008.
101. S. Ghosh, M. Tarafder, S. Sivaprasad, and S. Tarafder. Experimental and numerical study of ball indentation for evaluation of mechanical properties and fracture toughness of structural steel. *T Indian I Metals*, 63 (2-3):617–621, 2010.
102. D.D. Awale, A.R. Ballal, M.M. Thawre, V.D. Vijayanand, J.G. Kumar, and G.V.P. Reddy. Microstructural investigation and mechanical properties evaluation using miniature specimen testing of various constituents of dissimilar weld joint. *J Nucl Mater*, 532, 2020.
103. T. Suresh Kumar, A. Nagesha, J. Ganesh Kumar, P. Parameswaran, and R. Sandhya. Influence of thermal aging on tensile and low cycle fatigue behavior of type 316LN austenitic stainless steel weld joint. *Metall Mater Trans A*, 49(8):3257–3273, 2018.
104. S. Nagaraju, J. GaneshKumar, P. Vasantharaja, M. Vasudevan, and K. Laha. Evaluation of strength property variations across 9Cr-1Mo steel weld joints using automated ball indentation (ABI) technique. *Mater Sci Eng A*, 695:199–210, 2017.
105. R. Pamnani, V. Karthik, T. Jayakumar, M. Vasudevan, and T. Sakthivel. Evaluation of mechanical properties across micro alloyed HSLA steel weld joints using Au-

tomated Ball Indentation. *Mater Sci Eng A*, 651:214–223, 2016.

106. R.V. Prakash, P. Dhaka, G.V. Prasad Reddy, and R. Sandhya. Understanding the fatigue response of small volume specimens through novel fatigue test methods – experimental results and numerical simulation. *Theor Appl Fract Mec*, 103, 2019.
107. R.V. Prakash, M. Thomas, A.R. Prakash, and C.K. Mukhopadhyay. Online acoustic emission monitoring of cyclic ball indentation testing - correlation with hysteresis area response. volume 28, pages 1629–1636. Elsevier B.V., 2020.
108. H.R. Ammar, F.M. Haggag, A.S. Alaboodi, and F.A. Al-Mufadi. Nondestructive measurements of flow properties of nanocrystalline Al-Cu-Ti alloy using automated ball indentation (abi) technique. *Mat Sci Eng A*, 729:477–486, 2018.
109. M. Puchnin, O. Trudonoshyn, O. Prach, and F. Pešlová. Comparison of abi technique and standard methods in measuring mechanical properties of aluminium al-aloys. *Manuf Technol*, 16(3):37–38, 2016.
110. F. Wang, J. Zhao, and N. Zhu. Constitutive equations and ann approach to predict the flow stress of ti-6al-4v alloy based on abi tests. *J Mater Eng Perform*, 25(11): 4875–4884, 2016.
111. O. Trudonoshyn, M. Puchnin, and O. Prach. Use of the abi technique to measure the mechanical properties of aluminium alloys: Effect of heat-treatment conditions on the mechanical properties of alloys. *Materiali in Tehnologije*, 50(3):427–431, 2016.
112. D.C. Patil, K. Venkateswarlu, S.A. Kori, G. Das, M. Das, S.N. Alhajeri, and T.G. Langdon. Mechanical property evaluation of an al-2024 alloy subjected to hpt processing. volume 63. Institute of Physics Publishing, 2014.
113. D.R. Barbadikar, A.R. Ballal, D.R. Peshwe, J. Ganeshkumar, K. Laha, and M.D. Mathew. A study on the effect of tempering temperature on tensile properties of p92 steel by automated ball indentation technique. volume 86, pages 910–918. Elsevier Ltd, 2014.
114. R.V. Kulkarni, K.V. Mani Krishna, S. Neogy, D. Srivastava, E. Ramadasan, R.S. Shriwastaw, B.N. Rath, N. Saibaba, S.K. Jha, and G.K. Dey. Mechanical properties of zr-2.5to heat treatments in α+ βphase field. *J Nucl Mater*, 451(1-3):300–312, 2014.
115. J. Brumek, B. Strnadel, and I. Dlouhý. New approach to stress-strain curve prediction using ball indentation test. volume 1, pages 1049–1054, 2011. ISBN 9780791844519.
116. J.G. Kumar, V.D. Vijayanand, and K. Laha. Finite element simulation of plastic deformation of 316ln stainless steel during automated ball indentation test. *J Test Eval*, 48(4), 2020.
117. B. Li, S. Zhang, J. Li, J. Wang, and S. Lu. Quantitative evaluation of mechanical properties of machined surface layer using automated ball indentation technique. *Mater Sci Eng A*, 773, 2020.
118. J. Ganesh Kumar and K. Laha. Influence of some test parameters on automated ball indentation test results. *Exp Tech*, 42(1):45–54, 2018.
119. M. Das, T.K. Pal, and G. Das. Use of portable automated ball indentation system to evaluate mechanical properties of steel pipes. *T Indian I Metals*, 65(2):197–203, 2012.
120. G.M. Castelluccio, A.A. Yawny, J.E. Perez Ipiña, and H.A. Ernst. In situ evaluation of tensile properties of heat-affected zones from welded steel pipes. *Strain*, 48(1):68–74, 2012.
121. X. Chen, Z. Liu, G. He, and H. Xie. A novel integrated tension-compression design for a mini split Hopkinson bar apparatus. *Rev Sci Instrum*, 85(3), 2014.
122. M. N. Gussev, R. H. Howard, K. A. Terrani, and K. G. Field. Sub-size tensile specimen design for in-reactor irradiation and post-irradiation testing. *Nucl Eng Des*, 320:298–308, 2017.
123. M. Hayakawa, E. Nakayama, K. Okamura, M. Yamamoto, and K. Shizawa. Development of micro-shear fatigue test and its application to single crystal of pure iron. In *Procedia Engineer*, volume 160, pages 167–174, 2016.
124. D. Holländer, D. Kulawinski, A. Weidner, M. Thiele, H. Biermann, and U. Gampe. Small-scale specimen testing for fatigue life assessment of service-exposed industrial gas turbine blades. *Int J Fatigue*, 92:262–271, 2016.
125. D. Holländer, D. Kulawinski, M. Thiele, C. Damm, S. Henkel, H. Biermann, and U. Gampe. Investigation of isothermal and thermo-mechanical fatigue behavior of the nickel-base superalloy IN738LC using standardized and advanced test methods. *Mat Sci Eng A-Struct*, 670:314–324, 2016.
126. N. Kashaev, M. Horstmann, V. Ventzke, S. Riekehr, and N. Huber. Comparative study of mechanical properties using standard and micro-specimens of base materials Inconel 625, Inconel 718 and Ti-6Al-4 v. *J Mater Res Technol*, 2(1):43–47, 2013.
127. K. Kumar, A. Pooleery, K. Madhusoodanan, R.N. Singh, A. Chatterjee, B.K. Dutta, and R.K. Sinha. Optimisation of thickness of miniature tensile specimens for evaluation of mechanical properties. *Mat Sci Eng A-Struct*, 675:32–43, 2016.
128. Y. Murase, J. Nagakawa, and N. Yamamoto. In-beam fatigue behavior of 20300 °c. *Fusion Eng Des*, 81(8-14 Part B):999–1003, 2006.

129. E. Nakayama, M. Fukumoto, M. Miyahara, K. Okamura, H. Fujimoto, K. Fukui, and T. Kitamura. Evaluation of local fatigue strength in spot weld by small specimen. *Fatigue Fract Eng Mater*, 33(5):267–275, 2010.
130. Q. Wang and W. Zhang. Fatigue life prediction of smooth and circular-hole specimens based on equivalent initial flaw size. In Wang Z. Zhang S., editor, *Proceedings of 2015 the 1st International Conference on Reliability Systems Engineering, ICRSE 2015*, pages 1–7, 2015. ISBN 9781467385565.
131. H. Sakasegawa, X. Chen, T. Kato, H. Tanigawa, M. Ando, J.W. Geringer, S. Ukai, and S. Ohtsuka. Strain evaluation using a non-contact deformation measurement system in tensile tests of irradiated F82H and 9Cr ODS steels. *Nucl Mater Energy*, 16:108–113, 2018.
132. W. Vandermeulen, J.-L. Puzzolante, and M. Scibetta. Understanding of tensile test results on small size specimens of certified reference material BCR-661. *J Test Eval*, 45(2):695–703, 2017.
133. D.O. Fernandino, R.E. Boeri, and J.M. Massone. Mechanism of damage of ferritic ductile iron, influence of matrix heterogeneity. *Mater Sci Forum*, 925: 288–295, 2018.
134. I.V. Lomakin, A.R. Arutyunyan, R.R. Valiev, F.A. Gadzhiev, and M.Y. Murashkin. Design and evaluation of an experimental technique for mechanical and fatigue testing of sub-sized samples. *Exp Mech*, 42(3): 261–270, 2018.
135. Z. Špirit, M. Chocholoušek, and M. Šíma. Mechanical testing of anisotropy in ODS steel tubes. In *IOP Conference Series: Materials Science and Engineering*, volume 179, 2017.
136. J-. H. Baek, T. S. Byun, S Maloy, and M Toloczko. Investigation of temperature dependence of fracture toughness in high-dose HT9 steel using small-specimen reuse technique. *J Nucl Mater*, 444(1-3): 206–213, 2014.
137. T.S. Byun, S.A. Maloy, and J.H. Yoon. Small specimen reuse technique to evaluate fracture toughness of high dose HT9 steel. In Sokolov M.A. Lucon E., editor, *ASTM Spec Tech Publ*, volume STP 1576, pages 121–142. ASTM International, 2015. ISBN 9780803175976.
138. G.M. Castelluccio, J.E.P. Ipiña, A.A. Yawny, and H.A. Ernst. Fracture testing of the heat affected zone from welded steel pipes using an in situ stage. *Eng Frac Mech*, 98(1):52–63, 2013.
139. E. Gaganidze and J. Aktaa. Use of the failure assessment diagram to deduce ductile fracture toughness of the RAFM steel EUROFER97. *Int J Pres Ves Pip*, 86 (6):345–350, 2009.
140. A. Hojna, F. Di Gabriele, H. Hadraba, R. Husak, I. Kubena, L. Rozumova, P. Bublikova, J. Kalivodova, and J. Matejicek. Fracture behaviour of the 14Cr ODS steel exposed to helium and liquid lead. *J Nucl Mater*, 490:143–154, 2017.
141. O. Kovarik, A. Janca, and J. Siegl. Fatigue crack growth rate in miniature specimens using resonance. *Int J Fatigue*, 102:252–260, 2017.
142. H. Kurishita, H. Kayano, M. Narui, M. Yamazaki, Y. Kano, and I. Shibahara. Effects of V-notch dimensions on charpy impact test results for differently sized miniature specimens of ferritic steel. *Mater T JIM*, 34 (11):1042–1052, 1993.
143. H. Kurishita, T. Yamamoto, T. Nagasaka, A. Nishimura, T. Muroga, and S. Jitsukawa. Fracture toughness of JLF-1 by miniaturized 3-point bend specimens with 3.3-7.0 mm thickness. *Mater Trans*, 45(3):936–941, 2004.
144. B.-S. Lee, J.-H. Hong, W.-J. Yang, M.-Y. Huh, and S.-H. Chi. Master curve characterization of the fracture toughness in unirradiated and irradiated RPV steels using full- and 1/3-size pre-cracked charpy specimens. *Int J Pres Ves Pip*, 77(10):599–604, 2000.
145. S. Mahalingam, P.E.J. Flewitt, and J.F. Knott. The ductile-brittle transition for nominally pure polycrystalline nickel. *Mat Sci Eng A-Struct*, 564:342–350, 2013.
146. K.K. Ray. Simpler estimation of fracture toughness during material development, process optimization and quality control of structural materials. *Mater Sci Forum*, 736:192–206, 2013.
147. M. Serrano, P. Fernández, and J. Lapeña. Fracture toughness evaluation of Eurofer97 by testing small specimens. In *ASTM Spec Tech Publ*, volume 1502 STP, pages 114–121. American Society for Testing and Materials, 2009. ISBN 9780803145061.
148. J. Wunder, A. Karl, A. Dwars, and A. Boehm. Instrumented impact test of duplex stainless steel miniature specimen. *Materialwiss Werkst*, 44(9):797–803, 2013.
149. A.V. Kravchuk, E.O. Kondryakov, O.V. Panasenko, and V.V. Kharchenko. Determination of the temperature dependences of the fracture energy components of specimens of various types in impact bending tests. *Strength Mater*, 49(6):809–817, 2017.
150. C. Ruggieri. A modified local approach including plastic strain effects to predict cleavage fracture toughness from subsize precracked Charpy specimens. *Theor Appl Fract Mec*, 105, 2020.
151. I. Černý, D. Mikulová, and I. Fürbacher. Fatigue strength and failure mechanisms of nitrided small parts of a 30CrMoV9 steel. *Mater Manuf Processes*, 26(1): 1–6, 2011.

152. T. Hirose, H. Tanigawa, M. Ando, A. Kohyama, Y. Katoh, and S. Jitsukawa. Small specimen test technology for evaluation of fatigue properties of fusion structural materials. *Mater Trans*, 42(3):389–392, 2001.
153. A. King, W. Ludwig, M. Herbig, J.-Y. Buffire, A.A. Khan, N. Stevens, and T.J. Marrow. Three-dimensional in situ observations of short fatigue crack growth in magnesium. *Acta Mater*, 59(17):6761–6771, 2011.
154. S. Nogami, W. Guan, M. Toyota, and A. Hasegawa. Fatigue life prediction of ferritic/martensitic steels based on universal slope equations and tensile properties obtained using small specimen. *Fusion Eng Des*, 125:330–336, 2017.
155. S. Nogami, T. Itoh, H. Sakasegawa, H. Tanigawa, E. Wakai, A. Nishimura, and A. Hasegawa. Study on fatigue life evaluation using small specimens for testing neutron-irradiated materials. *J Nucl Sci Technol*, 48(1):60–64, 2011.
156. S. Nogami, A. Nishimura, E. Wakai, H. Tanigawa, T. Itoh, and A. Hasegawa. Development of fatigue life evaluation method using small specimen. *J Nucl Mater*, 441(1-3):125–132, 2013.
157. S. Nogami, Y. Sato, A. Tanaka, A. Hasegawa, A. Nishimura, and H. Tanigawa. Effect of specimen shape on the low cycle fatigue life of reduced activation ferritic/martensitic steel. *J Nucl Sci Technol*, 47 (1):47–52, 2010.
158. S. Nogami, W. Guan, M. Toyota, and A. Hasegawa. Fatigue life prediction of ferritic/martensitic steels based on universal slope equations and tensile properties obtained using small specimen. *Fusion Eng Des*, 125:330–336, 2017.
159. A. Ballesteros, V.A. Strizhalo, E.U. Grinik, L.S. Novogrudskii, L.I. Chirko, and M.P. Zemtsov. Determination of reference temperature T_0 for steel JRQ in an unirradiated state and construction of a master curve. *Strength Mater*, 34(1):27–34, 2002.
160. R. Kasada, H. Ono, and A. Kimura. Small specimen test technique for evaluating fracture toughness of blanket structural materials. *Fusion Eng Des*, 81 (8-14 PART B):981–986, 2006.
161. Y. Lin, W. Yang, Z. Tong, and G. Ning. Fracture toughness analysis of the china RPV steel with miniaturized specimen. *Mater Sci Forum*, 850:41–46, 2016.
162. C-. S. Shin and S-. W. Lin. Evaluating fatigue crack propagation properties using miniature specimens. *Int J Fatigue*, 43:105–110, 2012.
163. M. A. Sokolov and E. Lucon. Influence of specimen size/type on the fracture toughness of five irradiated RPV materials. In *17th International Conference on Environmental Degradation of Materials in Nuclear Power Systems – Water Reactors*, 2015.
164. K. Wallin. Validity of small specimen fracture toughness estimates neglecting constraint corrections. Number 1244, pages 519–537. ASTM, Philadelphia, PA, United States, 1995.
165. Z. Zhou, Z. Tong, G. Qian, and F. Berto. Specimen size effect on the ductile-brittle transition reference temperature of A508-3 steel. *Theor Appl Fract Mec*, 104, 2019.
166. W. Han, K. Yabuuchi, R. Kasada, A. Kimura, E. Wakai, H. Tanigawa, P. Liu, X. Yi, and F. Wan. Application of small specimen test technique to evaluate fracture toughness of reduced activation ferritic/martensitic steel. *Fusion Eng Des*, 125:326–329, 2017.
167. M. Yamamoto, K. Onizawa, K. Yoshimoto, T. Ogawa, Y. Mabuchi, M. Valo, M. Lambrecht, H.-W Viehrig, N. Miura, and N. Soneda. International round robin test on master curve reference temperature evaluation utilizing miniature c(t) specimen. *ASTM Special Technical Publication*, pages 53–69, 01 2015.
168. E. Lucon and M. Scibetta. Miniature compact tension specimens for upper shelf fracture toughness measurements on rpv steels. *J ASTM Int*, 5, 03 2008.
169. Y.S. Kim, Yu.G. Matvienko, and H.C. Jeong. Development of experimental procedure based on the load separation method to measure the fracture toughness of Zr-2.5Nb tubes. *Key Eng Mat*, 345-346 I:449–452, 2007.
170. Z. Xinping, S. Yaowu, and H. Ningshuang. The studies on fracture toughness of nuclear pressure vessel steels by using a small round compact tension specimen and a comparison with a Charpy-size specimen. *Int J Pres Ves Pip*, 69(2):169–174, 1996.
171. T. Kato, M. Ohata, S. Nogami, and H. Tanigawa. Evaluation of impacts of stress triaxiality on plastic deformability of RAFM steel using various types of tensile specimen. *Fusion Eng Des*, 109(B):1631–1636, 2016.
172. S. Nogami, C. Hisaka, M. Fujiwara, E. Wakai, and A. Hasegawa. High temperature fatigue life evaluation using small specimen. *Plasma Fusion Res*, 12: 1405022–1405022, 2017.
173. P.S. De, C.M. Obermark, and R.S. Mishra. Development of a reversible bending fatigue test bed to evaluate bulk properties using sub-size specimens. *J Test Eval*, 36(4):402–405, 2008.
174. P.S. De, R.S. Mishra, and C.B. Smith. Effect of microstructure on fatigue life and fracture morphology in an aluminum alloy. *Scripta Mater*, 60(7):500–503, 2009.
175. A. S. Haidyrah, J. W. Newkirk, and C. H. Castaño. Weibull statistical analysis of Krouse type bending fatigue of nuclear materials. *J Nucl Mater*, 470:244 –

250, 2016.

176. T. Sugimoto, T. Itoh, M. Sakane, and C. Hisaka. Development of fatigue testing machine for small sized specimen in liquid environment. *Key Eng Mat*, 734: 185–193, 2017.
177. J. Džugan, R. Prochazka, and P. Konopik. *Micro-Tensile Test Technique Development and Application to Mechanical Property Determination*. 05 2015. ISBN 978-0-8031-7597-6.
178. M. Hayakawa, M. Wakita, and E. Nakayama. Damage evaluation of ferrite and ferrite/pearlite steel during fatigue crack initiation by EBSD. In G Clark and CH Wang, editors, *11th International Fatigue Congress, Pts 1 and 2*, volume 891-892 of *Advanced Materials Research*, pages 410–415, 2014. ISBN 978-3-03835-008-8.
179. T. Nozawa, H. Ogiwara, J. Kannari, H. Kishimoto, and H. Tanigawa. Torsion test technique for interfacial shear evaluation of F82H RAFM HIP-joints. *Fusion Eng Des*, 86(9-11):2512–2516, 2011.
180. T. Nozawa, S. Noh, and H. Tanigawa. Determining the shear fracture properties of HIP joints of reduced-activation ferritic/martensitic steel by a torsion test. *J Nucl Mater*, 427(1-3):282–289, 2012.
181. C. Bao, L.X. Cai, and C. Dan. Estimation of fatigue crack growth behavior for small-sized C-shaped inside edge-notched tension (CIET) specimen using compliance technique. *Int J Fatigue*, 81:202–212, 2015.
182. S. Knitel, P. Spätig, and H.P. Seifert. An inverse method based on finite element model to derive the plastic flow properties from non-standard tensile specimens of Eurofer97 steel. *Nucl Mater Energy*, 9 (Supplement C):311 – 316, 2016.
183. S.-I. Komazaki, R. Jojima, N. Muraoka, S. Nogami, M. Kamaya, C. Hisaka, M. Fujiwara, and A. Nitta. Development of small bulge fatigue testing technique using small disk-type specimen. *Fatigue Fract Eng Mater*, 43(3):444–456, 2019.
184. H. Wang, T. Xu, and B. Shou. Determination of material strengths by hydraulic bulge test. *Materials*, 10 (1):23, 2017.
185. S. Jitsukawa, M. Kizaki, A. Umino, K. Shiba, and A. Hishinuma. Methods and devices for small specimen testing at the japan atomic energy research institute. In Anon, editor, *ASTM Spec Tech Publ*, number 1204, pages 289–307, 1993. ISBN 0803118694.
186. M. M. Parvez, Y. Chen, and F. Liou. Comparison of fatigue performance between additively manufactured and wrought 304l stainless steel using a novel fatigue test setup. 01 2020.
187. M. Gussev. Role of scale factor during tensile testing of small specimens. *ASTM Spec Tech Publ*, 6:1–19, 01 2014.
188. J. Volák and Z. Bunda. Comparison of selected fatigue characteristics of P92 steel and 15CH2NMFA steel. In *METAL 2016 - 25th Anniversary International Conference on Metallurgy and Materials, Conference Proceedings*, pages 885–890, 2016. ISBN 9788087294673.
189. J. Kazakeviciute, J.P. Rouse, D.S.A. De Focatiis, and C.J. Hyde. The development of a novel technique for small ring specimen tensile testing. *Theor Appl Fract Mec*, 99:131–139, 2019.
190. H. Zhu, S. Kumai, T. Tanaka, and A. Sato. Tear toughness evaluation of a permanent mold cast a356 aluminum alloy using a small-size specimen. *Mater Trans*, 45(5):1714–1721, 2004.
191. Y. Ito, M. Saito, K. Abe, and E. Wakai. Effect of hydrogen on crack growth behavior in F82H steel using small-size specimen. In Sokolov M.A. Lucon E., editor, *ASTM Spec Tech Publ*, volume STP 1576, pages 209–224, 2015. ISBN 9780803175976.
192. G. Chen, S-. C. Shan, X. Chen, and H. Yuan. Ratcheting and fatigue properties of the high-nitrogen steel X13CrMnMoN18-14-3 under cyclic loading. *Comp Mater Sci*, 46(3):572–578, 2009. ISSN 0927-0256.
193. European Committee for Standardization. *Small punch test method for metallic materials*. European Committee for Standardization, 2007. CEN Workshop Agreement,CWA 15627:2007 E.
194. *ASTM E3205-20, Standard Test Method for Small Punch Testing of Metallic Materials*. ASTM International, West Conshohocken, PA, 2020.
195. British Standards Institution. *BS EN 10371 Metallic materials. Small punch test method*. British Standards Institution, 2019.
196. Standards Press of China (SPC). *Small punch test methods of metallic materials for in-service pressure equipments –part 1: General requirements*. Standards Press of China (SPC), 2012.
197. Standards Press of China (SPC). *Small punch test methods of metallic materials for in-service pressure equipments –part 2: Method of test for tensile properties at room temperature*. Standards Press of China (SPC), 2012.
198. The Society of Materials Science. *Standard for small punch creep test – estimation of residual life for high temperature component*. The Society of Materials Science, Japan, 2012.
199. ASTM International. *ASTM E2248-18, Standard Test Method for Impact Testing of Miniaturized Charpy V-notch Specimens*. ASTM International, West Conshohocken, PA, 2018.
200. ASTM International. *ASTM E2546-15 Standard Practice for Instrumented Indentation Testing*. ASTM International, West Conshohocken, PA, 2015.

201. International Organization for Standardization. *BS EN ISO 14577-1:2015 Metallic materials. Instrumented indentation test for hardness and materials parameters. Test method*. International Organization for Standardization, 2015.
202. ASTM International. *ASTM E384-17 Standard Test Method for Microindentation Hardness of Materials*. ASTM International, West Conshohocken, PA, 2017.
203. B.J. Kim, R. Kasada, and A. Kimura. Effects of chemical composition on the impact properties of A533B steels. *Mater Sci Forum*, 654-656:2895–2898, 2010.
204. B.J. Kim, R. Kasada, A. Kimura, and H. Tanigawa. Evaluation of grain boundary embrittlement of phosphorus added F82H steel by SSTT. *J Nucl Mater*, 421 (1-3):153–159, 2012.
205. Y.-C. Kim, K.-H. Kim, and D. Kwon. Nondestructive mechanical property assessment using instrumented indentation testing. In *Proceedings of the International Offshore and Polar Engineering Conference*, volume 4, pages 312–315, 2010. ISBN 9781880653777.
206. S.W. Kim, H. Tanigawa, T. Hirose, and A. Kohyama. Effects of surface morphology and distributed inclusions on the low cycle fatigue behavior of miniaturized specimens of F82H steel. In *ASTM Spec Tech Publ*, volume 1502 STP, pages 159–169, 2009. ISBN 9780803145061.
207. B.J. Kim, R. Kasada, A. Kimura, and H. Tanigawa. Effects of specimen size on fracture toughness of phosphorous added F82H steels. *Fusion Eng Des*, 86(9-11):2403–2408, 2011.
208. B.J. Kim, R. Kasada, A. Kimura, and H. Tanigawa. Specimen size effects on fracture toughness of F82H steel for fusion blanket structural material. *Green Energy Technol*, 66:286–291, 2011.
209. R.K. Nanstad, M.A. Sokolov, and X. Chen. Fracture toughness of 9Cr-1MoV and thermally aged alloy 617 for advanced reactor applications. In *TMS Annual Meeting*, pages 343–356, 2012. ISBN 9781118291382.
210. M.-C. Kim, Y.J. Oh, and B.S. Lee. Evaluation of ductile-brittle transition temperature before and after neutron irradiation for RPV steels using small punch tests. *Nucl Eng Des*, 235(17-19):1799–1805, 2005.
211. K. Kapoor, N. Saibaba, B.P. Kashyap, and A.V. Ramana Rao. Tearing crack growth and fracture micromechanisms under micro segregation in Zr-2.5%Nb pressure tube material. *J ASTM Int*, 5(7), 2008.